$\mathcal{PT}$-symmetric quantum sensing: Advantages and restrictions

Yan-Yi Wang,[1,2,3,*] Chun-Wang Wu,[1,3,†] Wei Wu,[1,3] and Ping-Xing Chen[1,3]
[1]*Institute for Quantum Science and Technology, College of Science, NUDT, Changsha 410073, Hunan, China*
[2]*College of Science, Guangxi University of Science and Technology, Liuzhou 545006, Guangxi, China*
[3]*Hunan Key Laboratory of Quantum Information Mechanism and Technology, NUDT, Changsha 410073, Hunan, China*

(Received 22 December 2023; accepted 24 May 2024; published 18 June 2024)

Quantum sensing utilizing unique quantum properties of non-Hermitian systems to realize ultraprecision measurements has been attracting increasing attention. However, the debate on whether non-Hermitian systems are superior to Hermitian counterparts in sensing remains an open question. Here, we investigate the quantum information in $\mathcal{PT}$-symmetric quantum sensing utilizing two experimental schemes based on the trapped-ion platform and explore the relationship between $\mathcal{PT}$-symmetric quantum sensors and quantum resources. It turns out that the existence of advantages of non-Hermitian quantum sensing heavily depends on additional information resources carried by the extra degrees of freedom introduced to construct $\mathcal{PT}$-symmetric quantum sensors. Moreover, the practical application of non-Hermitian quantum sensing with superior performance is primarily restricted by the extra resource consumption accompanied by the postselection, while the superiority of non-Hermitian quantum sensing can be efficiently achieved in the presence of reasonable quantum resources. Our study provides theoretical references for the efficient construction of non-Hermitian quantum sensors with superior performance based on quantum resources and has potential applications in the research field of quantum precision measurement.

DOI: 10.1103/PhysRevA.109.062611

I. INTRODUCTION

In conventional quantum mechanics, the fundamental assumption of Hermiticity guarantees the reality of the eigenvalues of Hamiltonians and the unitarity of the time evolution of quantum systems. However, in the last two decades, *non-Hermitian* (NH) quantum mechanics has received considerable attention. Bender and Boettcher proposed that $\mathcal{PT}$-symmetric systems possessing non-Hermiticity can maintain real and positive energy spectra [1,2] and redefined the $\mathcal{PT}$ inner product [3]. $\mathcal{PT}$-symmetric systems can also be reinterpreted as a NH subsystem embedded into a larger Hermitian system [4–7]. Mostafazadeh further introduced pseudo-Hermiticity and explored a more general sense of $\mathcal{PT}$ symmetry [8,9]. The development of NH physics has been greatly propelled by the proposal of $\mathcal{PT}$ symmetry, and its applications have been widely extended across various research branches of quantum science and technology [10–12]. Particularly, the *exceptional point* (EP) of a $\mathcal{PT}$-symmetric Hamiltonian involves a switch in the eigenvalues from real to complex accompanying the degeneracy of the eigenstates [13–15], in consequence, $\mathcal{PT}$ symmetry is spontaneously broken. Hence, the EP-induced degeneracy (coalescence with criticality [16]), caused by the sensitivity divergence of the eigenenergy spectral gap [17], becomes one of the most striking characteristics of NH systems [18–20], and the observation of $\mathcal{PT}$-symmetry spontaneous breaking has been realized in various experimental works [21–24]. Recent studies, both in theory [25–28] and experiment [17,29,30], have reported that the EP can enhance both quantum and (quasi-) classical sensing [31].

Quantum sensing (QS) combined with precision measurement and quantum physics exploits unique quantum features to achieve ultraprecision measurement [32,33]. Within the framework of quantum theory, developing precise measurement methods to surpass the limitations of classical techniques by leveraging quantum resources is currently one of the main goals in this research field. In the last dozen years, QS has made rapid development in various systems [34], including single photon [35,36], cold atoms [37,38], trapped ions [39,40], superconducting qubits [41], and solid-state spins [42,43]. Our study is based on the trapped-ion platform, which has certain advantages such as long coherence time, multiple vibrational modes, strong robustness against environmental disturbances, and high connectivity between qubits, making it suitable for QS [39]. Recently, a debate has emerged regarding whether NH physics is superior in sensing. Except for the studies of *EP-enhanced quantum sensing* (EPQS) [17,25–30], some investigations also reported that sensors possessing unique NH characteristics have improved performance [44–48]. While some research suggested that the reported performance improvement might not have taken a full account of the effects of introduced noise [49–53], other works also indicated that the improved performance could exist even considering noise [54–57]. A recent study proposed that when comparing the performance of quantum sensors, it is essential to fix the quantum resources consumed by these sensors [58]. As far as we know, few studies have considered

*Contact author: wangyy@gxust.edu.cn
†Contact author: cwwu@nudt.edu.cn

that, on the premise of superior sensing performance, the advantages of *non-Hermitian quantum sensing* (NHQS) may be restricted by certain factors in practical applications, such as plenty of potential resource consumption with low efficiency. In light of the foregoing, we conduct a study to explore the condition under which the superiority of NHQS exists, investigate the additional quantum resource requirements accompanying the performance improvement of NHQS, and determine the corresponding resource utilization rate when the superiority of NHQS is present.

In this paper, based on two schemes of quantum simulations of $\mathcal{PT}$-symmetric systems, we verify that the EP does indeed significantly amplify the population shift as a response to the perturbation of the estimated parameter, which seems to be exploited to improve QS performance. However, we also observe that the EP may not always enhance susceptibility regarding the estimated parameter, and non-Hermiticity may reduce the susceptibility even without involving the EP. We further explore the relationship between $\mathcal{PT}$-symmetric quantum sensors and quantum resources, and demonstrate that the advantages of NHQS over its counterpart, *Hermitian quantum sensing* (HQS), deeply depend on whether the extra degrees of freedom introduced to construct $\mathcal{PT}$-symmetric systems carry additional quantum information. Moreover, the restrictions on practically improving performance in NHQS mainly arise from postselection involving additional resource consumption in realistic constructions of $\mathcal{PT}$-symmetric systems, while within the framework of resource theory, EPQS does indeed possess potential superiority, as its resource utilization rate can periodically reach 100% with the sensitivity bound achieving zero. This work has a potential promotion to develop quantum precision measurement.

The paper is organized as follows. In Sec. II, two schemes of quantum simulations of the $\mathcal{PT}$-symmetric system based on the trapped-ion platform are briefly introduced. In Sec. III, $\mathcal{PT}$-symmetric EPQS is verified by the population shift and susceptibility, and the advantages and restrictions of NHQS are investigated by the *quantum Fisher information* (QFI) and sensitivity bound. In Sec. IV, the superior performance of NHQS is discussed from the perspective of resource theory. Finally, conclusions and outlook are given in Sec. V.

II. $\mathcal{PT}$-SYMMETRIC QUANTUM SYSTEM

The $\mathcal{PT}$-symmetric quantum system, of which energy is balanced with gain ($|1\rangle$) and loss ($|2\rangle$), is governed by a NH Hamiltonian:

$$H_{\mathcal{PT}} = \frac{\omega}{2}\sigma_x + \mathrm{i}\frac{\gamma}{2}\sigma_z, \tag{1}$$

where ω and γ are the coupling rate and tunable gain-loss rate, $\sigma_{x,y,z}$ are Pauli matrices with $\sigma_z = |1\rangle\langle 1| - |2\rangle\langle 2|$, and $\mathrm{E}_\pm = \pm\kappa/2$ with $\kappa = \sqrt{\omega^2 - \gamma^2}$ are the eigenvalues of $H_{\mathcal{PT}}$ (the eigenvectors $|\mathrm{E}_\pm\rangle$ accord with the standard Dirac inner product). The ratio γ/ω usually quantifies the non-Hermiticity in the system. When $\gamma/\omega \in (0, 1)$, $H_{\mathcal{PT}}$ is in the $\mathcal{PT}$-symmetric phase and $\gamma/\omega = 1$ is regarded as the EP of $H_{\mathcal{PT}}$ [13,14], while $\gamma = 0$ denotes an absence of non-Hermiticity and the $\mathcal{PT}$-symmetric system degrades into a Rabi oscillator. Generally, NH dynamics is nonunitary due to the non-Hermiticity in the system, and the trace-preserving dynamics generated by a NH Hamiltonian $H_{\mathrm{NH}} = H_+ + H_-$ (with $H_\pm = \pm H_\pm^\dagger$ and $H_- = -\mathrm{i}\Gamma$) [59] ($\hbar = 1$) is

$$\dot{\rho}_t = -\mathrm{i}[H_+, \rho_t] - \{\Gamma, \rho_t\} + 2\mathrm{Tr}(\rho_t\Gamma)\rho_t, \tag{2}$$

where ρ_t is a normalized density operator. The solution of Eq. (2) can also be simply expressed as

$$\rho_t = \frac{U_{\mathcal{PT}}\rho_0 U_{\mathcal{PT}}^\dagger}{\mathrm{Tr}(U_{\mathcal{PT}}\rho_0 U_{\mathcal{PT}}^\dagger)}, \tag{3a}$$

where $U_{\mathcal{PT}} = \exp(-\mathrm{i}H_{\mathcal{PT}}t)$. Considering an initial pure state $\rho_0 = |\psi_0\rangle\langle\psi_0|$, Eq. (3a) is reduced to

$$|\psi_t\rangle = \frac{U_{\mathcal{PT}}|\psi_0\rangle}{\sqrt{\langle\psi_0|U_{\mathcal{PT}}^\dagger U_{\mathcal{PT}}|\psi_0\rangle}} = \mathrm{c_n}U_{\mathcal{PT}}|\psi_0\rangle, \tag{3b}$$

with the normalized factor $\mathrm{c_n} = (\langle\psi_0|U_{\mathcal{PT}}^\dagger U_{\mathcal{PT}}|\psi_0\rangle)^{-1/2}$. Note that although the mathematical form of Eq. (3) is unitarylike, both $U_{\mathcal{PT}}$ and the corresponding NH dynamics are still nonunitary in the standard Dirac sense. The major distinction between conventional (Hermitian) and $\mathcal{PT}$ quantum mechanics is the definition of the inner product; hence the $\mathcal{PT}$ inner product, whose associated norm is positive definite, is introduced for making sense of $\mathcal{PT}$ quantum mechanics [2,3]. To be clear and concise, we set the experiment-dependent parameter $\omega \to 1$ with the corresponding period of dynamics $T = 2\pi/\omega \to 2\pi$ and scale the evolution time with $\tau = \kappa t$ in subsequent numerical calculations and plots.

On the other hand, within the framework of standard quantum mechanics, realizing a NH Hamiltonian in a single quantum system poses quite a challenge. Currently, the primary approach for quantum simulation of the $\mathcal{PT}$-symmetric Hamiltonians involves introducing extra degrees of freedom, such as an auxiliary system [22,36,60–63] [Scheme I in Fig. 1(a)] or an external environment [23,24,40,64] [Scheme II in Fig. 1(b)]. For the first one, based on the Naimark-dilation theory and the postselection techniques, a $\mathcal{PT}$-symmetric system can be reinterpreted as a subspace in a larger Hilbert space [4], and the $\mathcal{PT}$-symmetric nonunitary dynamics is equivalent to the unitary dynamics in enlarged Hilbert space. For the other one, an open quantum system, whose dynamics obeys the Lindblad master equation, is dominated by an effective NH Hamiltonian when quantum jumps are ignored in the Lindbladian dissipator [14]. The experimental studies [63–65] have determined that the trapped-ion platform is feasible in realizing a $\mathcal{PT}$-symmetric system based on these schemes. In the following, two schemes for simulating the $\mathcal{PT}$-symmetric system will be briefly introduced (for more details, see Appendixes A and B). To facilitate reading, relevant systems in this paper, along with their corresponding abbreviations and symbols, are listed in Table I, and the correlations between these systems are shown in Fig. 1(c).

Scheme I: Naimark-dilated quantum system. Utilizing the Naimark-dilation theory, the $\mathcal{PT}$-symmetric system can be regarded as a NH subsystem embedded into a larger Hermitian system, which is achieved by embedding the $\mathcal{PT}$-symmetric subspace $\mathcal{H}_{\mathcal{PT}}$ into a larger Hermitian space $\mathcal{H}_{\mathrm{H(4d)}} = \mathcal{H}_{\mathcal{PT}(2\mathrm{d})} \oplus \mathcal{H}_{\mathcal{A}(2\mathrm{d})}$ with an auxiliary subspace $\mathcal{H}_{\mathcal{A}}$ [4] by constructing a Hermitian metric operator $\eta = \eta^\dagger$ based on

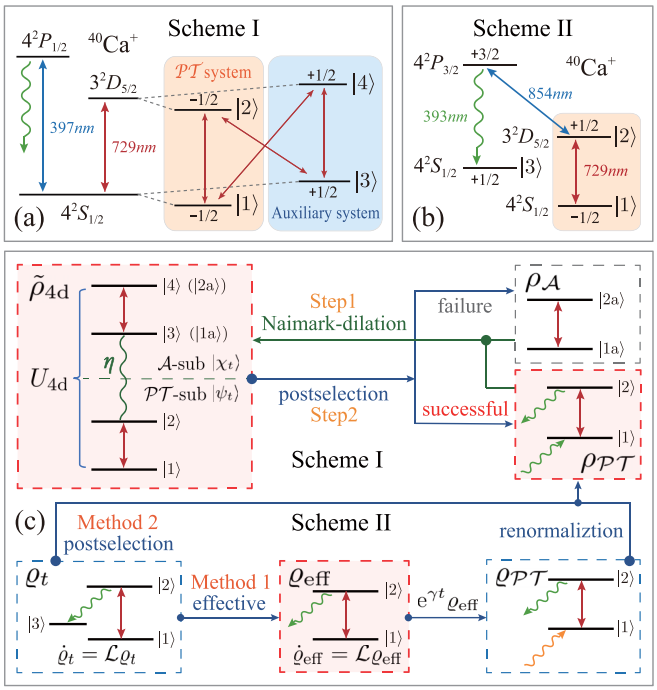

FIG. 1. Experimental schemes of quantum simulations of the $\mathcal{PT}$-symmetric system based on a trapped ion. (a) Scheme I with the digital quantum simulation method: Choosing Zeeman sublevels of the trapped $^{40}Ca^+$ ion as $|1\rangle = |4^2S_{1/2}(m_J = -1/2)\rangle$, $|2\rangle = |3^2D_{5/2}(m_J = -1/2)\rangle$, $|3\rangle = |4^2S_{1/2}(m_J = +1/2)\rangle$, and $|4\rangle = |3^2D_{5/2}(m_J = +1/2)\rangle$. Any S-D transition (red lines) can be implemented by a resonance drive using a 729-nm laser. Another 397-nm laser is used for cooling and fluorescence detection. Initial-state preparation and arbitrary unitary operation can be decomposed into appropriate sequences of S-D equatorial rotation $R(\theta, \phi) = \exp[-i\theta(\cos\phi\,\sigma_x^m + \sin\phi\,\sigma_y^m)/2]$, where θ and ϕ are the rotation angle and laser phase, and $\sigma_{x,y}^m$ are Pauli matrices [63]. (b) Scheme II with the analog quantum simulation method: Choosing Zeeman sublevels of the trapped $^{40}Ca^+$ ion as $|1\rangle = |4^2S_{1/2}(m_J = -1/2)\rangle$, $|2\rangle = |3^2D_{5/2}(m_J = +1/2)\rangle$, and $|3\rangle = |4^2S_{1/2}(m_J = +1/2)\rangle$. The trapped $^{40}Ca^+$ ion is initially prepared in $|1\rangle$ and then is resonantly driven to $|2\rangle$ by a 729-nm laser, and an 854-nm laser induces a tunable loss in $|2\rangle$ through coupling $|2\rangle$ to a short-life level $|4^2P_{3/2}(m_J = +3/2)\rangle$ which quickly decays to $|3\rangle$. Another 393-nm laser is used for cooling and fluorescence detection [64]. (c) Correlations between systems in this paper, details are given in Appendixes.

TABLE I. Symbols and corresponding quantum systems.

System (Abbr.)	Symbols
$\mathcal{PT}$-symmetric system	ρ_t, $\rho_{\mathcal{PT}}$
Enlarged Hermitian system	$\tilde{\rho}_{4d}$, $\|\Psi_t\rangle$
Auxiliary system ($\mathcal{A}$ system)	$\rho_{\mathcal{A}}$
$\mathcal{PT}$-symmetric subsystem ($\mathcal{PT}$-sub)	$\|\psi_t\rangle$
Auxiliary subsystem ($\mathcal{A}$-sub)	$\|\chi_t\rangle$
Dissipative two-level system	ϱ_{eff}, ρ_{eff}
Three-level system	ϱ_t
Artificial $\mathcal{PT}$-symmetric system	$\varrho_{\mathcal{PT}}$

the pseudo-Hermiticity condition $\eta H_{\mathcal{PT}} = H_{\mathcal{PT}}^\dagger \eta$ [9]. With the basis $\{|i\rangle\}$ $(i = 1, 2, 3, 4)$, the $\mathcal{PT}$-symmetric subsystem ($\mathcal{PT}$-sub) $|\psi_t\rangle$ is denoted with $\{|1\rangle, |2\rangle\}$, and the auxiliary subsystem ($\mathcal{A}$-sub) $|\chi_t\rangle$ is denoted with $\{|3\rangle, |4\rangle\}$. Obeying the $\mathcal{PT}$ inner product $(\mu, \nu) = (\mathcal{PT}\mu)\nu$ [3], the eigenvectors $|E_\pm\rangle$ of $H_{\mathcal{PT}}$ satisfy that $(E_\pm, E_\mp) = 0$ and $(E_\pm, E_\pm) = \pm 1$. Arranging them as $\Phi = (|E_+\rangle\,|E_-\rangle)$, the dimensionless metric operator is defined by

$$\eta = (\Phi\Phi^\dagger)^{-1} = \frac{1}{\kappa}(\gamma\sigma_y + \mathbb{I}), \tag{4}$$

which is considered as a synchronization link of dynamics between $\mathcal{A}$-sub $|\chi_t\rangle$ and $\mathcal{PT}$-sub $|\psi_t\rangle$,

$$|\chi_t\rangle = \eta|\psi_t\rangle, \tag{5}$$

and the enlarged Hermitian system is constructed as

$$|\Psi_t\rangle = \mathrm{C_n}\left(\begin{bmatrix}1\\0\end{bmatrix} \otimes |\psi_t\rangle + \begin{bmatrix}0\\1\end{bmatrix} \otimes |\chi_t\rangle\right) = \mathrm{C_n}\begin{pmatrix}\psi_t\\ \chi_t\end{pmatrix}, \tag{6}$$

where $\mathrm{C_n} = 1/\sqrt{\langle\psi_t|\psi_t\rangle + \langle\chi_t|\chi_t\rangle}$ is a normalized factor, and $\tilde{\rho}_{4d} = |\Psi_t\rangle\langle\Psi_t|$ represents the normalized density operator of enlarged Hermitian system with the initial state $\tilde{\rho}_0 = |\Psi_0\rangle\langle\Psi_0|$ related to $|\Psi_0\rangle = (\psi_0\ \chi_0)^{\mathrm{T}}$, where $|\chi_0\rangle = \eta|\psi_0\rangle$ is the initial state of $\mathcal{A}$-sub and $|\psi_0\rangle$ for $\mathcal{PT}$-sub. The corresponding time-evolution operator is

$$U_{\mathrm{H}} = \begin{pmatrix} U_{\mathcal{PT}} & 0 \\ 0 & \eta U_{\mathcal{PT}} \eta^{-1}\end{pmatrix}, \tag{7}$$

and then Eq. (6) can be expressed in $|\Psi_t\rangle = U_{4d}|\Psi_0\rangle$, where $U_{4d} = (\mathrm{C_n c_n})U_{\mathrm{H}} = \exp(-iH_{4d}t)$. Now, with the Naimark-dilation theory, we have obtained the unitary time-evolution operator $U_{4d}U_{4d}^\dagger = \mathbb{I}$ associated with the Hermitian Hamiltonian $H_{4d} = H_{4d}^\dagger$, and the corresponding unitary time evolution $\tilde{\rho}_{4d} = U_{4d}\tilde{\rho}_0 U_{4d}^\dagger$. Populations in the state $|i\rangle$ $(i = 1, 2, 3, 4)$ of the enlarged Hermitian system $\tilde{\rho}_{4d}$, represented by the matrix diagonal elements $P_{i(t)} = \tilde{\rho}_{4d}^{ii}$, are exhibited in Figs. 2(a) and 2(b), in which $|1\rangle$ for $\mathcal{PT}$-sub and $|3\rangle$ for $\mathcal{A}$-sub.

Considering the postselection, we can obtain the normalized population for $\mathcal{PT}$-sub:

$$\tilde{P}_1 = \frac{P_1}{P_1 + P_2}; \quad \tilde{P}_2 = \frac{P_2}{P_1 + P_2}, \tag{8a}$$

and the corresponding normalized population for $\mathcal{A}$-sub:

$$\tilde{P}_3 = \frac{P_3}{P_3 + P_4}; \quad \tilde{P}_4 = \frac{P_4}{P_3 + P_4}. \tag{8b}$$

If the postselection is executed successfully, the enlarged Hermitian system with $P_{i(t)} = \tilde{\rho}_{4d}^{ii}$ $(i = 1, 2)$ in Eq. (8a) would collapse to the $\mathcal{PT}$-symmetric system with $p_{i(t)} = \rho_t^{ii}$ $(i = 1, 2)$, where ρ_t^{ii} are the matrix diagonal elements of ρ_t in Eq. (3a). The success rate and failure rate of postselection are respectively denoted as $p_{\text{suc}} = P_1 + P_2$ and $p_{\text{fail}} = 1 - p_{\text{suc}}$, shown in Figs. 2(c) and 2(d). After executing the postselection, normalized density matrices of the $\mathcal{PT}$-symmetric system $\rho_{\mathcal{PT}}$ and auxiliary system ($\mathcal{A}$ system) $\rho_{\mathcal{A}}$ are respectively degraded into

$$\rho_{\mathcal{PT}} = \rho_t = \frac{|\psi_t\rangle\langle\psi_t|}{\mathrm{Tr}(|\psi_t\rangle\langle\psi_t|)} = \begin{pmatrix}\rho_t^{11} & \rho_t^{12}\\ \rho_t^{21} & \rho_t^{22}\end{pmatrix}, \tag{9a}$$

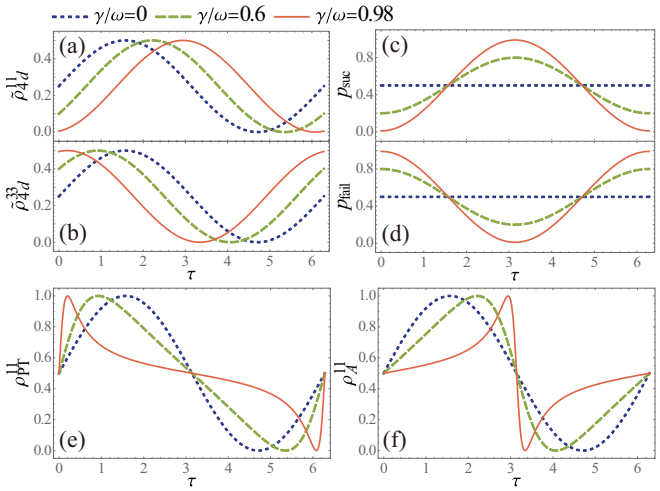

FIG. 2. Populations and related quantities vs the scaled evolution time $\tau = \kappa t$ for different non-Hermiticity γ/ω with the initial conditions $|\psi_0\rangle = |+\rangle_y$ and $|\Psi_0\rangle = (\psi_0\, \eta\psi_0)^{\mathrm{T}}$. Population of subsystems in enlarged Hermitian system before the postselection: (a) $\mathcal{PT}$-sub $\tilde{\rho}_{4d}^{11}$, and (b) $\mathcal{A}$-sub $\tilde{\rho}_{4d}^{33}$. Related quantities of the postselection: (c) success rate p_{suc}, and (d) failure rate p_{fail}. Population of systems after the postselection: (e) $\mathcal{PT}$-symmetric system $\rho_{\mathcal{PT}}^{11}$, and (f) $\mathcal{A}$ system $\rho_{\mathcal{A}}^{11}$.

where ρ_t^{ij} $(i, j = 1, 2)$ with $|\psi_0\rangle = |+\rangle_y$, and

$$\rho_{\mathcal{A}} = \frac{|\chi_t\rangle\langle\chi_t|}{\mathrm{Tr}(|\chi_t\rangle\langle\chi_t|)} = \begin{pmatrix} \rho_t^{22} & \rho_t^{21} \\ \rho_t^{12} & \rho_t^{11} \end{pmatrix}, \tag{9b}$$

where ρ_t^{ij} $(i, j = 1, 2)$ with $|\psi_0\rangle = |-\rangle_y$, and the pure states $|\pm\rangle_y = (|1\rangle \pm \mathrm{i}|2\rangle)/\sqrt{2}$ are the eigenvectors of the Pauli matrix σ_y. Population in $|1\rangle$ of $\rho_{\mathcal{PT}}$ and $\rho_{\mathcal{A}}$ are exhibited in Figs. 2(e) and 2(f), respectively.

Note that the $\mathcal{PT}$-symmetric system (or $\mathcal{A}$ system) obtained from executing the postselection is different from the $\mathcal{PT}$-sub (or $\mathcal{A}$-sub) in the enlarged Hermitian system. The former one possessing trace-preserving dynamics is obtained by executing the postselection on the enlarged Hermitian system; the latter one is without performing the postselection, of which dynamics is not trace preserving. Although the $\mathcal{PT}$-sub (or $\mathcal{A}$-sub) placed in the subspace of the larger Hermitian space possesses non-trace-preserving dynamics, the enlarged Hermitian system retains trace-preserving dynamics. Additionally, Eq. (9) indicates that $\mathcal{A}$-sub does indeed possess the $\mathcal{PT}$ symmetry due to the synchronization link η with $\mathcal{PT}$-sub, and consequently the EPs of $\mathcal{PT}$-sub and $\mathcal{A}$-sub are overlapping. The interlaced dynamics behavior shown in Figs. 2(e) and 2(f) also demonstrates that two subsystems possess an anti-mirror-symmetric correlation, and the enlarged Hermitian system is combined by two synchronized $\mathcal{PT}$-symmetric subsystems (i.e., the enlarged Hermitian system can be regarded as a pseudo-dual-$\mathcal{PT}$-symmetric system). More details of Scheme I are given in Appendix A.

Scheme II: Effective non-Hermitian Hamiltonian of open quantum system. $\mathcal{PT}$ symmetry requires an exact energy balance of gain and loss, which is challenging to achieve within the quantum realm. Coupling Hermitian systems with a dissipative reservoir can overcome this obstacle [18,21]. Considering a dissipative two-level system (i.e., an open quantum system), whose energy is only with loss ($|2\rangle$) and without gain ($|1\rangle$), is described by an effective NH Hamiltonian with the basis $\{|i\rangle\}$ $(i = 1, 2)$:

$$H_{\mathrm{eff}} = \frac{\omega}{2}\sigma_x - \mathrm{i}\gamma|2\rangle\langle 2| = H_{\mathcal{PT}} - \mathrm{i}\frac{\gamma}{2}\mathbb{I}, \tag{10}$$

where $H_{\mathcal{PT}}$ is given by Eq. (1). The dissipative two-level system can also be expressed as a three-level system [24], the coherent transition is denoted by $|1\rangle \leftrightarrow |2\rangle$ with the coupling rate ω, the loss of the system is represented by $|2\rangle \to |3\rangle$ with the tunable decay rate γ, and $|1\rangle \nleftrightarrow |3\rangle$. The dynamics of the three-level system obeys the Lindblad master equation with a Liouvillian superoperator $\mathcal{L}$:

$$\dot{\varrho}_t = \mathcal{L}\varrho_t = -\mathrm{i}[H_0, \varrho_t] + \left(J\varrho_t J^\dagger - \tfrac{1}{2}\{J^\dagger J, \varrho_t\}\right), \tag{11}$$

where $H_0 = \omega\sigma_x/2$ is the coherent transition Hamiltonian, and $J = \sqrt{\gamma}\,|3\rangle\langle 2|$ is the jump operator. The dynamics of the dissipative two-level system governed by H_{eff} can be determined by a lower-dimension (3D $\to$ 2D) Lindblad master equation reduced from Eq. (11):

$$\dot{\varrho}_{\mathrm{eff}} = \mathcal{L}\varrho_{\mathrm{eff}} = -\mathrm{i}[H_{\mathrm{eff}}, \varrho_{\mathrm{eff}}], \tag{12}$$

where ϱ_{eff} is a non-normalized density operator of the dissipative two-level system. Equation (12) indicates that the lower-dimension superoperator $\mathcal{L}$ without quantum jumps plays the same role as the effective NH Hamiltonian H_{eff} in the dissipative dynamics. The solution of Eq. (12) can also be simply expressed as

$$\varrho_{\mathrm{eff}} = U_{\mathrm{eff}}\varrho_0 U_{\mathrm{eff}}^\dagger, \tag{13}$$

where $U_{\mathrm{eff}} = \exp(-\mathrm{i}H_{\mathrm{eff}}t)$. Equation (13) can be reduced to $\varrho_{\mathrm{eff}} = |\psi_{\mathrm{eff}}\rangle\langle\psi_{\mathrm{eff}}|$ and $|\psi_{\mathrm{eff}}\rangle = U_{\mathrm{eff}}|\psi_0\rangle$ for initial pure states $\varrho_0 = \rho_0 = |\psi_0\rangle\langle\psi_0|$. In the practical experiment [64], the directly measured quantity is

$$\varrho_{\mathcal{PT}} = \mathrm{e}^{\gamma t}\varrho_{\mathrm{eff}}, \tag{14}$$

where $\mathrm{e}^{\gamma t}$ denotes the gain term, which is artificially added to simulate the characteristic of energy balance between gain and loss in the $\mathcal{PT}$-symmetric system, and $\varrho_{\mathcal{PT}}$ can be renormalized as

$$\rho_{\mathcal{PT}} = \frac{\varrho_{\mathcal{PT}}}{\mathrm{Tr}(\varrho_{\mathcal{PT}})} = \frac{\mathrm{e}^{\gamma t}\varrho_{\mathrm{eff}}}{\mathrm{Tr}(\mathrm{e}^{\gamma t}\varrho_{\mathrm{eff}})} = \frac{\varrho_{\mathrm{eff}}}{\mathrm{Tr}(\varrho_{\mathrm{eff}})} = \rho_{\mathrm{eff}}. \tag{15a}$$

Equation (15a) indicates that after the renormalization, both $\varrho_{\mathcal{PT}}$ and ϱ_{eff} degrade into the normalized $\rho_t = \rho_{\mathcal{PT}} = \rho_{\mathrm{eff}}$ in Eq. (3a); hence the effective NH Hamiltonian of the dissipative two-level system can be used to equivalently describe the $\mathcal{PT}$-symmetric system. From the perspective of the postselection [24], $\rho_{\mathcal{PT}}$ can also be obtained by directly performing the postselection on ϱ_t:

$$\rho_{\mathcal{PT}} = \frac{1}{\varrho_t^{11} + \varrho_t^{22}} \begin{pmatrix} \varrho_t^{11} & \varrho_t^{12} \\ \varrho_t^{21} & \varrho_t^{22} \end{pmatrix} = \begin{pmatrix} \rho_t^{11} & \rho_t^{12} \\ \rho_t^{21} & \rho_t^{22} \end{pmatrix}, \tag{15b}$$

where ϱ_t^{ij} $(i, j = 1, 2, 3)$ are matrix elements of ϱ_t given by solving Eq. (11), $p_{\mathrm{suc}} = \varrho_t^{11} + \varrho_t^{22}$ is the success rate of postselection, and ρ_t^{ij} $(i, j = 1, 2)$ are matrix elements of ρ_t in Eq. (3a). The population of artificial $\mathcal{PT}$-symmetric system $\varrho_{\mathcal{PT}}$ and dissipative two-level system ϱ_{eff} with $|\psi_0\rangle = |+\rangle_y =$

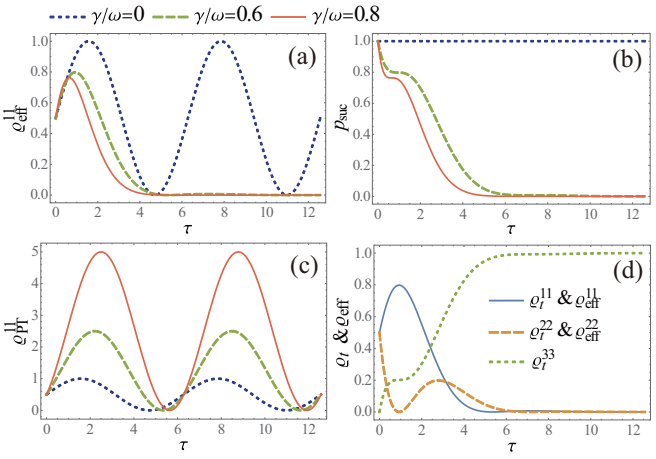

FIG. 3. Populations and related quantities vs τ for different γ/ω with the initial condition $|\psi_0\rangle = |+\rangle_y$: (a) dissipative two-level system $\varrho_{\rm eff}^{11}$; (b) success rate $p_{\rm suc}$ of the postselection for dissipative two-level system $\varrho_{\rm eff}$; (c) artificial $\mathcal{PT}$-symmetric system $\varrho_{\mathcal{PT}}^{11}$; (d) population of $|i\rangle$ in three-level system ϱ_t and the corresponding dissipative two-level system $\varrho_{\rm eff}$ with $\gamma/\omega = 0.6$.

$(|1\rangle + i|2\rangle)/\sqrt{2}$ (i.e., three-level system ϱ_t with $|\tilde{\psi}_0\rangle = |\tilde{+}\rangle_y = (|1\rangle + i|2\rangle + 0|3\rangle)/\sqrt{2}$) are respectively exhibited in Figs. 3(c) and 3(d).

After executing the renormalization or postselection, the dissipative dynamics in Fig. 3(a) would degrade into the $\mathcal{PT}$-symmetric dynamics in Fig. 2(e), which shows that constructing the $\mathcal{PT}$-symmetric system by introducing an environment can also be regarded as a kind of method of expanding dimension (e.g., 2D → 3D). However, the steady state of a dissipative two-level system is associated with a vanishing success rate, as shown in Figs. 3(b) and 3(d), indicating that such an expansion will be broken under prolonged evolution. Besides, the Liouvillian superoperator $\mathcal{L}$, expressed by a NH matrix, possesses EPs which can be defined by the degeneracy points of $\mathcal{L}$ eigenmatrices [14]. It can be easily determined that at $\gamma/\omega = 1$, the *Hamiltonian exceptional point* (HEP) of $H_{\mathcal{PT}}$ in Eq. (1) coincides with the *Liouvillian exceptional point* (LEP) of $\mathcal{L}$ in Eq. (12). More details of Scheme II are given in Appendix B.

III. $\mathcal{PT}$-SYMMETRIC QUANTUM SENSING

In Sec. III A, based on the two schemes mentioned above, we first examine (i) population shift and (ii) susceptibility, to verify whether the EP can potentially enhance QS. And then, in Sec. III B we discuss (iii) the condition for existing advantages of NHQS over HQS by using QFI and a sensitivity bound, and investigate (iv) whether the postselection imposes restrictions on improving the performance of NHQS.

A. $\mathcal{PT}$-symmetric EP-enhanced quantum sensing

Quantum sensing achieves ultraprecision sensing by using the unique quantum properties of $\mathcal{PT}$-symmetric systems, such as the eigenstates coalescence and the susceptibility divergence at the EP, which is called EPQS.

1. Population shift with respect to the perturbation of estimated parameter

Population shift is considered a response to the perturbation of the estimated parameter and directly reflects the ability to distinguish population change under the perturbation. From the perspective of quantum parameter estimation, the estimated parameter is directly coupled to the degrees of freedom of the system, and the introduced parameter-dependent perturbation can be represented by a Hermitian Hamiltonian:

$$H_1 = \frac{\delta}{2}\sigma_x. \tag{16}$$

Generally, the perturbation amplitude δ is rather weak, and the parameter-dependent $\mathcal{PT}$-symmetric Hamiltonian under the perturbation is

$$\tilde{H}_{\mathcal{PT}(\omega)} = H_{\mathcal{PT}} + H_1 = \frac{\Omega}{2}\sigma_x + i\frac{\gamma}{2}\sigma_z, \tag{17}$$

with $\Omega = \omega + \delta$. Equations (1) and (10) are accordingly modified as $\omega \to \Omega$ and $H_{\mathcal{PT}} \to \tilde{H}_{\mathcal{PT}}$, and the coupling rate ω is the parameter to be estimated. The population shifts of $|1\rangle$ related to the estimated-parameter perturbation δ for different systems are shown in Fig. 4. It can be observed that near the EP ($\gamma/\omega = 1 - 10^{-5}$), even a tiny perturbation ($\delta/\omega = 0.1\%$ and 0.5%) can lead to a significant population shift depicted by red curves, but the population shift of Hermitian counterpart ($\gamma = 0$) does not respond to the perturbation, which indicates that the $\mathcal{PT}$-symmetric system (before introducing extra degrees of freedom) and the systems of two schemes (after introducing auxiliary system or external environment) are all extremely sensitive to the estimated-parameter perturbation near the EP. Based on this, the EP has the potential to enhance QS. The main mechanism of the EP-enhanced response of perturbation is the strong dependency of energy-level splitting on the parameter near the EP [15]. The derivative of eigenvalues and eigenvectors with respect to the estimated parameter diverges at EP, which is also one of the fundamental distinctions between NH and Hermitian Hamiltonians. However, eigenvalue variations under the perturbation may not be an applicable measure of the comprehensive sensing performance at the EP [53]. To further comprehend the EP-enhanced response, the susceptibility concerning the estimated parameter would be considered.

2. Susceptibility with respect to the estimated parameter

Susceptibility quantifies how sensitively the population would respond to the variation of estimated parameter. It is defined by the derivative of the normalized population in $|i\rangle$ of the parameterized state ρ_ω with respect to the estimated parameter ω, because the normalized population would become extremely sensitive to the parameter at certain measurement points with a given evolution time [27], and it can also be directly obtained by taking the derivative of population with respect to ω:

$$S_\omega = \partial_\omega \rho_\omega^{ii}, \tag{18}$$

where ρ_ω^{ii} is the ith diagonal element of the corresponding parameter-dependent density matrix ρ_ω. Usually, the maximum susceptibility corresponds to the optimal measurement point.

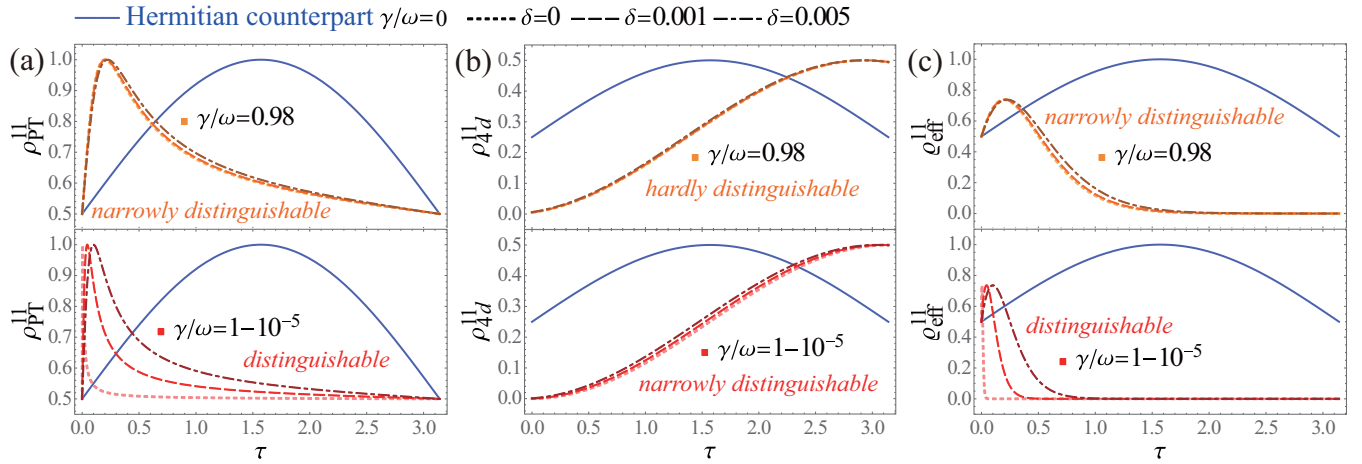

FIG. 4. Population shift with respect to the perturbation of estimated parameter δ vs τ for different γ/ω: (a) $\mathcal{PT}$-symmetric system $\rho_{\mathcal{PT}}$ [i.e., ρ_t in Eq. (3a)]; (b) enlarged Hermitian system $\tilde{\rho}_{4d}$; and (c) dissipative two-level system ρ_{eff}.

For Scheme I, $S_\omega^{\mathcal{PT}}$ of the $\mathcal{PT}$-symmetric system shown in Fig. 5(a) exhibits a divergent feature in the vicinity of the EP ($\gamma/\omega = 0.99$) and possesses a sensitive response to the perturbation ($\delta/\omega = 0.1\%$, thinner curves). It can be anticipated that the EP divergence of susceptibility appears having the potential to achieve sensing with arbitrary precision. And $S_\omega^{\mathcal{A}}$ of $\mathcal{A}$ system, shown in Fig. 5(b), is consistent with $S_\omega^{\mathcal{PT}}$ and also presents a divergent feature and sensitive response in the vicinity of the EP. From the perspective of the enlarged Hermitian system, Figs. 5(c) and 5(d) show that although S_ω^{4d} exhibits a similar pattern of EP divergence and sensitive response as that of the $\mathcal{PT}$-symmetric system, both the speed and intensity of the EP divergence are noticeably restrained and weakened. This primarily results from two systems connected by the synchronization link η, which possess interlaced evolution behavior of S_ω [in Figs. 5(a) and 5(b)]. This also leads to an internal constraint between $\mathcal{PT}$-sub and $\mathcal{A}$-sub, thereby weakening the EP divergence.

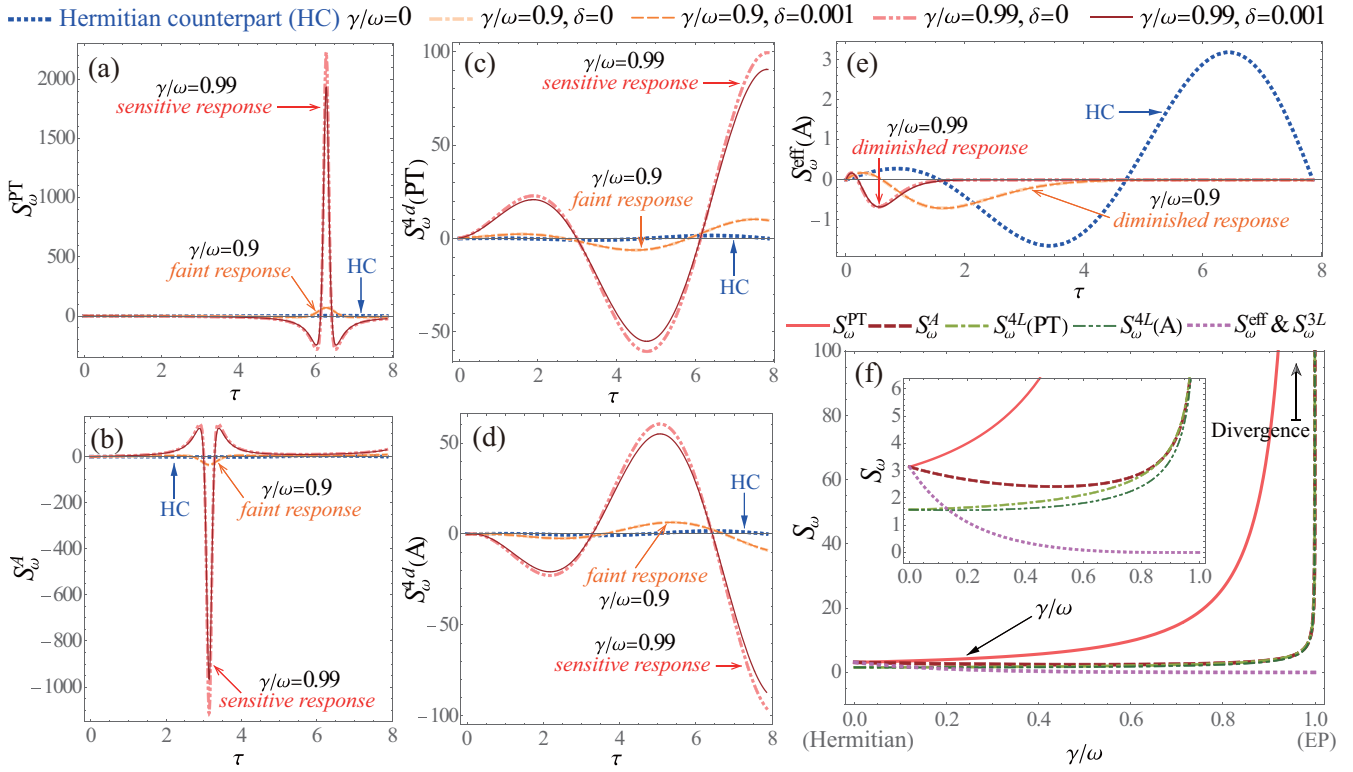

FIG. 5. Susceptibility S_ω in Eq. (18) with respect to the estimated parameter ω vs τ for different γ/ω and the perturbation δ. (a)–(d) For Scheme I: (a) $\mathcal{PT}$-symmetric system $\rho_{\mathcal{PT}}$, $S_\omega^{\mathcal{PT}} = \partial_\omega \rho_{\mathcal{PT}}^{11}$; (b) $\mathcal{A}$ system $\rho_{\mathcal{A}}$, $S_\omega^{\mathcal{A}} = \partial_\omega \rho_{\mathcal{A}}^{11}$; (c) $\mathcal{PT}$-sub (represented equivalently to enlarged Hermitian system with $\tilde{\rho}_{4d}^{11}$ in this sense), $S_\omega^{\text{4d}}(\mathcal{PT}) = \partial_\omega \tilde{\rho}_{4d}^{11}$; (d) $\mathcal{A}$-sub, $S_\omega^{\text{4d}}(\mathcal{A}) = \partial_\omega \tilde{\rho}_{4d}^{33}$. (e) For Scheme II: Dissipative two-level system ϱ_{eff}, $S_\omega^{\text{eff}} = \partial_\omega \varrho_{\text{eff}}^{11}$ (i.e., three-level system $\varrho_t^{11} = \varrho_{\text{eff}}^{11}$, $S_\omega^{\text{3L}} = \partial_\omega \varrho_t^{11}$). (f) Susceptibility $S_\omega = \partial_\omega \rho_\omega^{ii}$ vs γ/ω for different parameterized states ρ_ω at $\tau = 2\pi$.

As for Scheme II, S_ω^{eff} of the dissipative two-level system does not diverge near the EP shown in Fig. 5(e), which is entirely different from that of the $\mathcal{PT}$-symmetric system. Instead, S_ω^{eff} approaches zero during prolonged evolution and shows little response to the perturbation. Particularly, S_ω^{eff} of the dissipative two-level system ($\gamma \neq 0$) is distinctly weaker compared to its Hermitian counterpart [$\gamma = 0$, blue-dotted curves in Fig. 5(e)]. In other words, the stronger the non-Hermiticity, the weaker S_ω^{eff} [violet-dotted curves in Fig. 5(f)], even if it presents a faint response to the perturbation. This contrasts with the superior feature observed in Scheme I, in which non-Hermiticity can dramatically enhance the susceptibility [red and green curves in Fig. 5(f)].

Consequently, the anticipation that the EP divergence of susceptibility can be used to achieve sensing with arbitrary precision is not necessarily accurate, since the EP may not always enhance the susceptibility with respect to the estimated parameter. On the contrary, the non-Hermiticity may reduce the susceptibility even without involving the EP. To explore the condition of existing the superiority of NHQS, we would further investigate QFI and sensitivity bound in quantum measurements.

B. Advantages and restrictions of non-Hermitian quantum sensing

As mentioned above, the debate on whether NHQS is superior to HQS remains ongoing. Here, a question is presented: What is the condition under which the superiority of NHQS exists? Supposing that NHQS indeed possesses superior sensing performance, it is necessary to consider whether the performance improvement comes with potential costs or losses.

1. Sensitivity of non-Hermitian quantum sensors

In quantum metrology, the sensitivity is represented by QFI, which is defined as the supremum of classical Fisher information and regarded as a measure of the precision of parameter estimation. The inverse of QFI sets the lower bound on the error of estimation [66]. In NH or open quantum systems, parameterized processes typically involve nonunitary dynamics, which can be mapped from unitary dynamics in larger systems, enabling the direct application of concepts such as QFI and sensitivity bound to parameter estimation based on such mapped dynamics [58]. With the symmetric logarithmic derivative (SLD),

$$\partial_\omega \rho_\omega = \tfrac{1}{2}(L_\omega \rho_\omega + \rho_\omega L_\omega), \tag{19}$$

the definition of QFI is given by

$$\mathcal{F}_\omega = \text{Tr}\big(\rho_\omega L_\omega^2\big), \tag{20a}$$

where L_ω is the SLD operator, and ρ_ω is an arbitrary parameterized state. With the spectral decomposition of a density matrix, $\rho_\omega = \sum_n \varepsilon_n |\psi_n\rangle\langle\psi_n|$, Eq. (20a) can be expanded in the eigenvector representation of ρ_ω:

$$\mathcal{F}_\omega = \sum_n \frac{(\partial_\omega \varepsilon_n)^2}{\varepsilon_n} + \sum_n 4\varepsilon_n \langle \partial_\omega \psi_n | \partial_\omega \psi_n \rangle - \sum_{n\neq m} \frac{8\varepsilon_n \varepsilon_m}{\varepsilon_n + \varepsilon_m} |\langle \partial_\omega \psi_n | \psi_m \rangle|^2. \tag{20b}$$

For a pure parameterized state $\rho_\omega = |\psi_\omega\rangle\langle\psi_\omega|$, Eq. (20b) can be reduced to $\mathcal{F}_\omega = 4(\langle \partial_\omega \psi_\omega | \partial_\omega \psi_\omega \rangle - |\langle \psi_\omega | \partial_\omega \psi_\omega \rangle|^2)$. Considering a general two-level system [66–68], the basis-independent expression of QFI can be explicitly obtained,

$$\mathcal{F}_\omega = \text{Tr}[(\partial_\omega \rho_\omega)^2] + \frac{1}{\det(\rho_\omega)} \text{Tr}[(\rho_\omega \partial_\omega \rho_\omega)^2], \tag{20c}$$

and Eq. (20c) can also be reduced to $\mathcal{F}_\omega = 2\text{Tr}[(\partial_\omega \rho_\omega)^2]$ for a pure ρ_ω. The channel QFI corresponding to the maximum achievable QFI is obtained by optimizing over all possible probe states. The optimal probe state is to always a pure state (see Appendix C) due to the convexity of QFI [69]. The inverse of channel QFI quantifies the sensitivity bound of parameter estimation,

$$\delta\omega \geqslant \frac{1}{\sqrt{N\mathcal{F}_\omega}}, \tag{21}$$

where N represents the repetitions of measurement, and Eq. (21) is the well-known quantum Cramèr-Rao bound.

Note that realistic constructions of $\mathcal{PT}$-symmetric systems necessitate a postselection involving a success rate; as a consequence, Eq. (20) characterizes the estimated-parameter information obtained from a single measurement, and Eq. (21) represents the corresponding sensitivity bound ($N = 1$). When performing repeated measurements, it is necessary to consider the success rate of postselection. By averaging the outcomes of repeated measurements, the information (i.e., QFI) obtained from a repeated-averaged measurement can be expressed. As for Scheme I, under the postselection, the weighted QFI $\mathcal{I}_\omega$ obtained from a repeated-averaged measurement for the $\mathcal{PT}$-symmetric system and $\mathcal{A}$ system are given as

$$\mathcal{I}_\omega^{\text{suc}} = \mathcal{F}_\omega^{\mathcal{PT}} p_{\text{suc}}, \tag{22a}$$

$$\mathcal{I}_\omega^{\text{fail}} = \mathcal{F}_\omega^{\mathcal{A}} p_{\text{fail}}, \tag{22b}$$

where $\mathcal{I}_\omega^{\text{suc}}$ represents QFI when the postselection is executed successfully, the other $\mathcal{I}_\omega^{\text{fail}}$ for failure. By summing $\mathcal{I}_\omega^{\text{suc}}$ and $\mathcal{I}_\omega^{\text{fail}}$, the total QFI obtained from a repeated-averaged measurement involving the success rate is

$$\mathcal{I}_\omega^{\text{subs}} = \mathcal{I}_\omega^{\text{suc}} + \mathcal{I}_\omega^{\text{fail}}. \tag{23a}$$

Without (or before) the postselection, the total QFI of the enlarged Hermitian system, uninvolved with the success rate, is directly represented by $\mathcal{F}_\omega$ in Eq. (20):

$$\mathcal{I}_\omega^{\text{4d}} = \mathcal{F}_\omega^{\text{4d}}. \tag{23b}$$

For Scheme II, the total QFI of a dissipative two-level system obtained from a repeated-averaged measurement is

$$\mathcal{I}_\omega^{\text{eff}} = \mathcal{F}_\omega^{\text{eff}} p_{\text{suc}}^{\text{eff}}, \tag{24}$$

where the success rate $p_{\text{suc}}^{\text{eff}} = \varrho_t^{11} + \varrho_t^{22}$ is denoted by the trace of ϱ_{eff}. The sensitivity bound represented by Eq. (21) is correspondingly modified with $\mathcal{F}_\omega \to \mathcal{I}_\omega$:

$$\delta\omega \geqslant \frac{1}{\sqrt{N\mathcal{I}_\omega}}. \tag{25}$$

In order to determine whether NHQS is superior to HQS, QFI $\mathcal{F}_\omega$, $\mathcal{I}_\omega$ and sensitivity bound $\delta\omega$ of the two schemes are contrastively exhibited in Fig. 6 with the optimal probe state

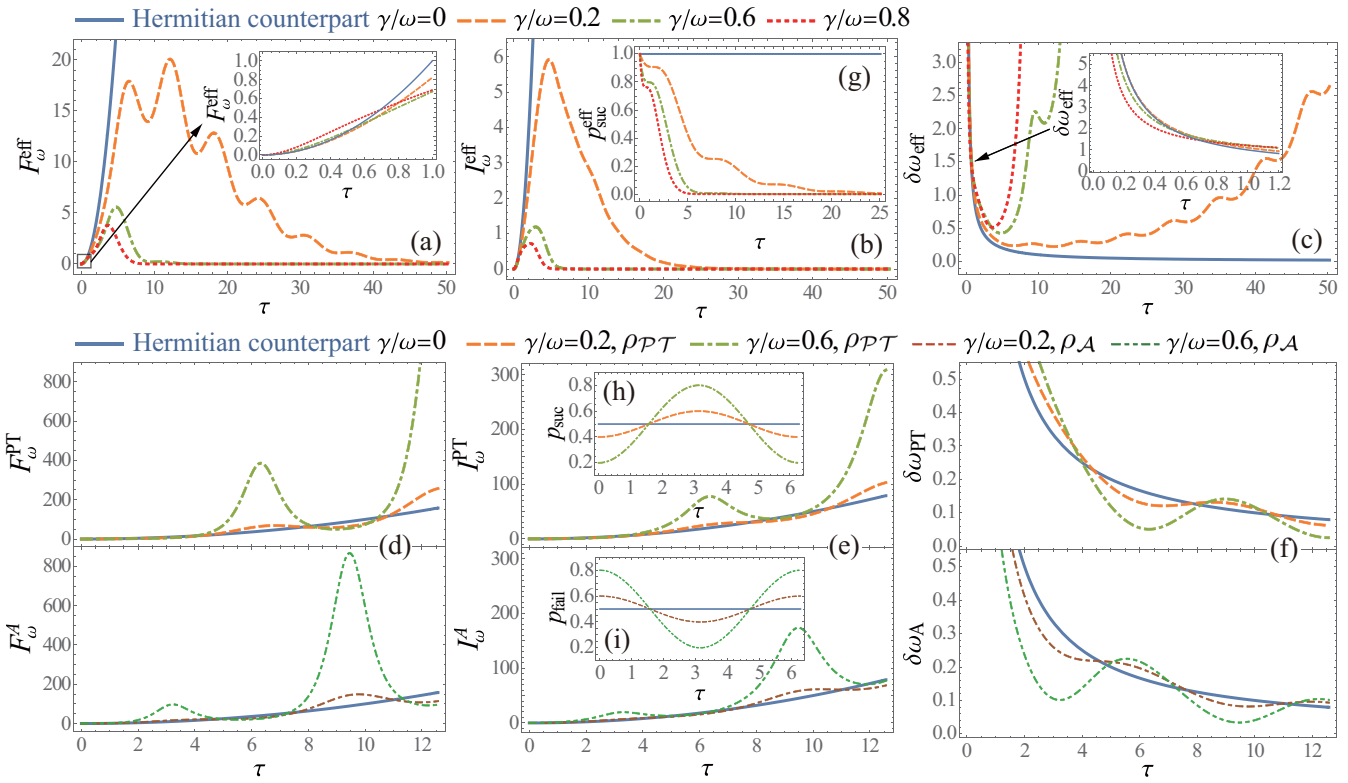

FIG. 6. QFI $\mathcal{F}_\omega$ in Eq. (20), $\mathcal{I}_\omega$ in Eqs. (22) and (24), and sensitivity bound $\delta\omega$ in Eq. (21) with respect to the estimated parameter ω vs τ for different γ/ω with the averaged-measure scale $N = 1$. (a)–(c) for Scheme II, dissipative two-level system ϱ_{eff}: (a) QFI with single successful measurement, $\mathcal{F}_\omega^{\text{eff}}$; (b) QFI with repeated-averaged measurement, $\mathcal{I}_\omega^{\text{eff}}$; (c) sensitivity bound with single successful measurement, $\delta\omega_{\text{eff}}$. (d)–(f) for Scheme I, $\mathcal{PT}$-symmetric system $\rho_{\mathcal{PT}}$ and $\mathcal{A}$ system $\rho_{\mathcal{A}}$ of enlarged Hermitian system under the postselection: (d) QFI with single measurement, $\mathcal{F}_\omega^{\mathcal{PT}}$ and $\mathcal{F}_\omega^{\mathcal{A}}$; (e) QFI with repeated-averaged measurement, $\mathcal{I}_\omega^{\mathcal{PT}}$ and $\mathcal{I}_\omega^{\mathcal{A}}$; (f) sensitivity bound with single measurement, $\delta\omega_{\mathcal{PT}}$ and $\delta\omega_{\mathcal{A}}$. Other related quantities with the same system parameters: (g) success rate $p_{\text{suc}}^{\text{eff}}$ of the postselection in dissipative two-level system ρ_{eff} for Scheme II; (h) success rate p_{suc} and (i) failure rate p_{fail} of the postselection in enlarged Hermitian system $\tilde{\rho}_{4\text{d}}$ for Scheme I.

$|\psi_0\rangle = |+\rangle_y$ (i.e., a pure initial state). Since the repetitions N in $\delta\omega$ of a NH system is the same as its Hermitian counterpart, we plot subsequent figures with the averaged-measure scale $N = 1$.

For Scheme II, Figs. 6(a) and 6(c) indicate that $\mathcal{F}_\omega^{\text{eff}}$ and $\delta\omega_{\text{eff}}$ of the dissipative two-level system ($\gamma \neq 0$) obtained from a single successful measurement are generally lower compared to their Hermitian counterparts ($\gamma = 0$), and slightly surpass Hermitian counterparts during the initial period only (shown in subfigures). The oscillatory evolution behavior of $\mathcal{F}_\omega^{\text{eff}}$ can be attributed to the simultaneous encoding and loss of estimated-parameter information in the parameterized process. And $\mathcal{F}_\omega^{\text{eff}}$ completely loses during prolonged evolution because the steady state does not contain any estimated-parameter information. This loss results from the non-Hermiticity (i.e., dissipation) in the dissipative two-level system jointed with the invariance of total estimated-parameter information in the parameterized process. In Fig. 6(b), $\mathcal{I}_\omega^{\text{eff}}$ involving the postselection appears to be at a notable decrease and accelerated loss compared to $\mathcal{F}_\omega^{\text{eff}}$, because the success rate gradually vanishes as $p_{\text{suc}}^{\text{eff}} \to 0$, shown in Fig. 6(g).

As for Scheme I, the synchronization link η connects subsystems of the enlarged Hermitian system and leads to the relevance of interlaced dynamics behaviors shown in Figs. 2(e) and 2(f) between the $\mathcal{PT}$-symmetric system and $\mathcal{A}$ system even after postselection. This relevance makes evolution behaviors of $\mathcal{F}_\omega^{\mathcal{PT}}$ and $\mathcal{F}_\omega^{\mathcal{A}}$ obtained from a single measurement in the $\mathcal{PT}$-symmetric system and $\mathcal{A}$ system also exhibit an interlaced pattern as shown in Fig. 6(d). Obviously, the introduced degrees of freedom of the $\mathcal{A}$ system equally carry the estimated-parameter information. Contrary to Scheme II, the presence of the non-Hermiticity ($\gamma \neq 0$) based on Scheme I significantly enhances $\mathcal{F}_\omega$ and $\delta\omega$ compared to the Hermitian counterparts ($\gamma = 0$), even in the absence of the EP. Considering a repeated-averaged measurement, Figs. 6(e) and 6(f) also show that, despite the success rate of postselection being oscillatory shown in Fig. 6(h), the non-Hermiticity indeed increases the information obtained from measurements and improves the corresponding sensitivity bound without involving the EP. In simple terms, for NHQS based on Scheme I, the stronger the non-Hermiticity, the higher the sensitivity, which means a superior QS performance, while NHQS based on Scheme II is inferior to HQS.

Consequently, the $\mathcal{A}$ system, introduced for practically constructing the $\mathcal{PT}$-symmetric system based on Scheme I, does indeed provide additional estimated-parameter information which actually enhances the coding ability of the parameter generator in the parameterized process. By comparison, based on Scheme II, the total estimated-parameter information remains invariant in the parameterized process, and the dissipative effect leads the information of the system

to flow into the external environment, and thereby the coding ability of the parameter generator is counteracted. This demonstrates that the advantages of NHQS over HQS deeply depend on the extra degrees of freedom introduced to construct NH quantum sensors whether they carry additional estimated-parameter information. Moreover, the effectiveness of the additional estimated-parameter information, derived from the extra degrees of freedom and represented by its capacity to be encoded into the parameterized state of the target $\mathcal{PT}$-symmetric system, contributes to enhancing the precision of parameter estimation.

In addition, a recent work presented a novel perspective on dissipative QFI based on the Liouvillian parameterized process [70]. The authors proposed that due to the fundamental differences in the quantum levels of HEP and LEP, with HEP being interpretable as a semiclassical limit of LEP, LEP provides a more accurate elucidation of the singularity of open systems compared to the HEP. This also explains why an EP does not always lead to an improvement in measurement precision. However, regardless of the measurement precision attainable near either HEP or LEP, the information obtained from measurements in a dissipative system is generally lower than that without dissipation and is completely lost during prolonged evolution. Although we calculated the conventional QFI of a dissipative system (in Scheme II) governed by an effective NH Hamiltonian in Eq. (10) whose HEP coincides with LEP, we focus on figuring out the potential physical mechanism that enhances the measurement precision of NH systems and exploring the restrictions on the performance improvement of NHQS (in Scheme I), which possesses superiority over HQS and may not necessarily involve the EP.

Another theoretical study recently proposed a general conclusion on the fundamental sensitivity limits for NH quantum sensors [58]; we also concur with their viewpoint that when comparing the performance of quantum sensors, it is necessary to fix the quantum resources consumed by these sensors. Hence, the Naimark-dilated ancilla system or the NH system considered in their study does not increase the amount of estimated-parameter information of the entire system during the parameterized process. As a result, ultraprecision parameter estimation, unsurprisingly, cannot be attained at the EP for their sample systems. Nevertheless, our work centers on investigating whether superior performance can exist in NHQS. We demonstrated that if the introduced degrees of freedom contain the estimated-parameter information, it will enhance the coding ability of the parameter generator during the parameterized process and make the superiority of NHQS present (as Scheme I); otherwise, it will weaken the parameter coding ability (as Scheme II). Based on this, we will further consider the quantum resources consumed in NHQS.

Of course, as we look forward to effectively improving the QS performance by utilizing the characteristics of NH quantum sensors, our attention would be devoted to Scheme I, which provides a superior indicator of sensitivity in NHQS. In the following, from the perspective of quantum resources, our goal is to determine whether there exists an additional requirement of information resources accompanied by the performance improvement of NHQS and to ascertain the corresponding resource utilization rate, which has a profound influence on practically taking advantage of NHQS.

2. Information costs and sensitivity losses related to the postselection

Within the framework of resource theory [71], resources are identified by certain quantum properties of systems. The benefits of these quantum resources are quantified for various quantum information processing tasks, and the difference in attainable tasks between those with and without the resources will be primarily considered. The notions of quantum parameter estimation have been introduced into the framework of resource theories and made significant progress, and all quantum resources have been proven to confer an advantage in metrology [72]. Since its clear physical meaning related to quantum fluctuation and favorable mathematical properties, QFI can be employed as a reliable resource measure [73]. In this context, QFI emerges as the most natural measure for connecting quantum resources with QS [33]. Based on conceptions of QFI $\mathcal{I}_\omega$ and sensitivity bound $\delta\omega$ in Eqs. (23) and (25), we introduce the following definitions. The information cost $\xi_{\mathcal{I}_\omega}$ is associated with the postselection and represents the utilization rate of information resources:

$$\xi_{\mathcal{I}_\omega} = \frac{\Delta\mathcal{I}_\omega}{\mathcal{I}_\omega^{4\mathrm{d}}} = \frac{\mathcal{I}_\omega^{4\mathrm{d}} - \mathcal{I}_\omega^{\mathrm{subs}}}{\mathcal{I}_\omega^{4\mathrm{d}}}, \tag{26}$$

where $\mathcal{I}_\omega^{\mathrm{subs}}$ corresponds to the presence of postselection, while $\mathcal{I}_\omega^{4\mathrm{d}}$ corresponds to the absence of postselection. According to the function of postselection, the lower the information cost $\xi_{\mathcal{I}_\omega}$ is, the less redundant information is required, which indicates more available estimated-parameter information encoded in the quantum state. $\xi_{\mathcal{I}_\omega} = 1$ represents that the postselection destroys the coding ability of the parameter generator and depletes all the information resources; $\xi_{\mathcal{I}_\omega} = 0$ denotes the absence of redundant information (i.e., the resource utilization rate is 100%). And the corresponding sensitivity loss related to the postselection is

$$\zeta_{\delta\omega} = \frac{\delta\omega_{4\mathrm{d}}}{\delta\omega_{\mathrm{subs}}} = \sqrt{\frac{\mathcal{I}_\omega^{\mathrm{subs}}}{\mathcal{I}_\omega^{4\mathrm{d}}}}. \tag{27}$$

The ratio of sensitivity bounds $\delta\omega_{4\mathrm{d}}$ and $\delta\omega_{\mathrm{subs}}$ directly demonstrates the sensitivity losses caused by the postselection: a lower $\zeta_{\delta\omega}$ indicates a higher utilization rate of resource consumption, and $\zeta_{\delta\omega} = 1$ represents the absence of sensitivity losses, while $\zeta_{\delta\omega} = 0$ is the sensitivity total loss (i.e., the resource utilization rate is 0%).

Focusing on Scheme I, which possesses superiority in QS, Fig. 7(a) indicates that QFI $\mathcal{I}_\omega^{\mathrm{subs}}$ (thicker, lighter curves) obtained from the measurements is indeed decreased by the postselection, compared with $\mathcal{I}_\omega^{4\mathrm{d}}$ (thinner, darker curves). Obviously, the stronger the non-Hermiticity, the larger QFI, but the more redundant information is required to be encoded into the parameterized state as shown in Fig. 7(c). Such an additional requirement of information distinctly increases resource consumption during the parameterized process, such as the extra energy usage [53], which poses an extra challenge for the practical implementation of ultraprecision NHQS and imposes restrictions on its practicable applications. Meanwhile, Fig. 7(b) shows that the postselection increases the costs of information resources and sensitivity losses. The stronger the non-Hermiticity, the more sensitivity loss shown in Fig. 7(d). Particularly, at EP ($\gamma/\omega = 1$), Fig. 7(e) shows that the

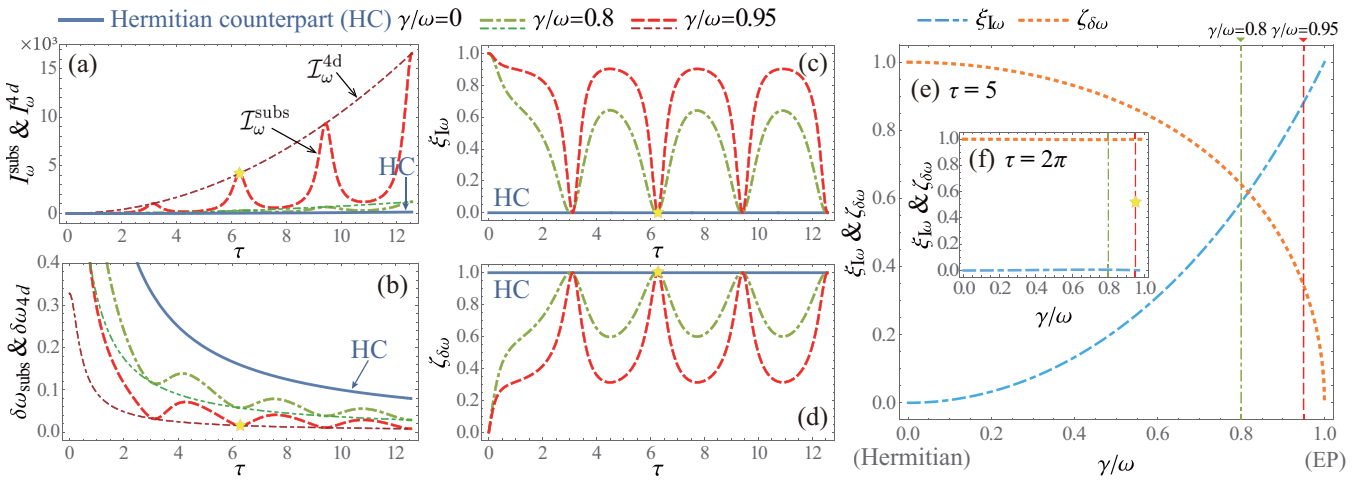

FIG. 7. QFI $\mathcal{I}_\omega$ in Eq. (23) and sensitivity bound $\delta\omega$ in Eq. (25) of Scheme I with respect to the estimated parameter ω vs τ for different γ/ω with the averaged-measure scale $N = 1$. Taking a repeated-averaged measurement: (a) comparison of QFI $\mathcal{I}_\omega^{\text{subs}}$ (thicker, lighter curves) and $\mathcal{I}_\omega^{\text{4d}}$ (thinner, darker curves); (b) comparison of sensitivity bound $\delta\omega_{\text{subs}}$ (thicker, lighter curves) and $\delta\omega_{\text{4d}}$ (thinner, darker curves). Performing the postselection: (c) information costs $\xi_{\mathcal{I}_\omega}$ in Eq. (26) vs τ for different γ/ω; (d) sensitivity losses $\zeta_{\delta\omega}$ in Eq. (27) vs τ for different γ/ω. Information costs $\xi_{\mathcal{I}_\omega}$ and sensitivity losses $\zeta_{\delta\omega}$ with the postselection vs γ/ω at (e) $\tau = 5$ and (f) $\tau = 2\pi$.

postselection depletes all information resources ($\xi_{\mathcal{I}_\omega} = 1$) and completely eliminates sensitivity ($\zeta_{\mathcal{I}_\omega} = 0$). This demonstrates that under the postselection, the resource utilization rate decreases to 0% at EP, which makes the superior performance of EPQS meaningless for practical applications. In simple terms, although the non-Hermiticity in the $\mathcal{PT}$-symmetric system indeed makes a superior performance of NHQS ($\gamma \neq 0$) over its Hermitian counterpart [$\gamma = 0$, blue curves in Figs. 7(a) and 7(b)], it unavoidably introduces more information resource requirements under the postselection.

It is easy to determine that the susceptibility $S_\omega = \partial_\omega \rho_\omega^{ii}$ in Eq. (18) corresponds to one of the diagonal elements of the SLD operator matrix $\partial_\omega \rho_\omega$ in Eq. (19). Meanwhile, the SLD operator is a crucial component in the definition of QFI in Eq. (20), which quantifies the sensitivity. The superior performance of NHQS is revealed by the precision of parameter estimation, which is improved by the non-Hermiticity without involving EP [in Fig. 6(f)], and the susceptibility diverges at EP [see Fig. 5(f)]. However, it seems counterintuitive that under the postselection the susceptibility diverges at EP, at which sensitivity is eliminated with a resource utilization rate of 0% [in Fig. 7(e)]. This contradiction can be attributed to the periodicity in the evolution behavior of the $\mathcal{PT}$-symmetric system. Particularly, by setting $\tau = 2\pi$, $\zeta_{\delta\omega} = 1$ [in Fig. 7(f)] can also be obtained even without involving the EP (star points of $\gamma/\omega = 0.95$ in Fig. 7), which instead indicates that the resource utilization rate is 100%. Note that the main objective here is to determine the potential costs or losses associated with the performance improvement of NHQS; hence we discussed the additional requirement of information resources without considering the special case of (half-) periodic points $\tau = n\pi$ ($n = 1, 2, 3 \ldots$).

Consequently, based on Scheme I, the practical implementation of performance improvement of NHQS is primarily restricted by the postselection related to the additional consumption of information resources accompanied by a low utilization rate, even if the $\mathcal{PT}$-symmetric quantum sensor possesses a superior indicator in QS.

IV. DISCUSSIONS

Undoubtedly, we do indeed expect the performance of QS to be effectively improved. If we can realize the superiority of NHQS with high efficiency and low consumption of quantum resources, why would we not?

In light of what has been discussed, we have to address the issue related to utilization rate, particularly concerning the additional energy usage involved in the practical construction of $\mathcal{PT}$-symmetric quantum sensors. Based on the effect of dissipation and quantum fluctuation, both Refs. [58,70] alleged that exceptional estimation precision cannot be attained at the EP for their models. It is obvious that the useful quantum resources required for ultraprecision metrology are compromised by the dissipation and decoherence in quantum systems. One of the results of our investigation demonstrates that the performance of NHQS can be enhanced by non-Hermiticity even in the absence of the EP. The superiority of NHQS derives from the extra degrees of freedom introduced to practically construct the $\mathcal{PT}$-symmetric system, carrying additional quantum resources. This is closely associated with the structure scheme of NH quantum sensors. Another significant finding of our investigation reveals that the practical application of NHQS based on Scheme I with superior performance is primarily restricted by the additional resource consumption accompanied by the postselection.

Notwithstanding the above, there indeed exists a noteworthy feature in EPQS, considering the periodic (half-periodic) points with a vanished success rate (failure rate) at the EP, a unique phenomenon arises: QFI diverges at the EP (i.e., the lower bound of parameter estimation error achieves zero) and the resource utilization rate reaches 100%. Except that the success (or failure) rate of postselection

periodically vanishes and the eigenstates coalesce at the EP, we further demonstrate that the mechanism behind this unique phenomenon is highly correlated with quantum resources. We unambiguously believe that if the amount of estimated-parameter information during the parameterized process does not increase, achieving NHQS with arbitrary precision at the EP under the quantum fluctuation and noise would be impossible. However, if the introduced degrees of freedom carry the additional estimated-parameter information, the statement would be inaccurate. Such as for non-Markovian dynamics, the estimated-parameter information is retrieved back from the environment to the system, and the presence of information flow would enhance the parameter estimation precision and the *signal-to-noise ratio* (SNR) of QS at the EP of a non-Markovian $\mathcal{PT}$-symmetric sensor [57]. The non-Markovianity represents a typical quantum resource in the nonconvex resource theories, and surpassing the limits set by quantum noise necessitates the utilization of quantum resources.

Nevertheless, in the absence of constraints on resource consumption, Hermitian systems can also achieve ultraprecision QS utilizing quantum resources, such as quantum entanglement. This is one core of the debate on whether NH systems outperform their Hermitian counterparts in sensing. In the scenario of reasonably providing an equal amount of quantum resources, NHQS will be superior to its counterpart HQS, since its resource utilization rate reaches 100% at periodic points that can be leveraged as optimal measurement points, which indicates that it is necessary to further evaluate the tradeoff between quantum precision measurement and quantum resources rather than merely estimate the superiority.

V. CONCLUSIONS AND OUTLOOK

In conclusion, we have investigated the advantages and restrictions of $\mathcal{PT}$-symmetric QS, utilizing two schemes based on the trapped-ion platform, and explored the relationship between $\mathcal{PT}$-symmetric quantum sensors and quantum resources. Our results show that the superior performance of NHQS depends on whether the extra degrees of freedom introduced to practically construct the $\mathcal{PT}$-symmetric system carry additional information resources. Moreover, in practical application, the advantages of NHQS are primarily restricted by the postselection introducing extra information resource requirements. However, NHQS does indeed possess potential superiority in the presence of extra quantum resources, attributed to its resource utilization rate achieving 100% at periodic points, while the lower bound of parameter estimation error reaches zero at the EP. This discovery is pivotal for realizing ultraprecision NHQS with high efficiency and low quantum resource consumption, which is worthwhile to further research; the relevant achievements will contribute to advancing the research field of quantum precision measurement.

$\mathcal{PT}$-symmetric systems have great research value in various application fields due to their quantum characteristics. Achieving high-fidelity quantum simulation of the $\mathcal{PT}$-symmetric system becomes a primary task to unlock its application potential. The comprehensive performance of quantum computers determines the accuracy and scope of quantum simulation, while the quantum simulation evaluates and verifies the quantum computing performance, and the trapped-ion system has emerged as one of the most promising candidates to realize quantum computation in the NISQ era. However, the fidelity of both experimental schemes mentioned above currently falls far short of the required standards for practical applications. To tackle the key challenges of quantum computation on trapped-ion systems in the NISQ era, we are diligently conducting a series of optimization studies on the comprehensive performance of a trapped-ion quantum computation platform. For the future, our industrious endeavors will focus on implementing the efficient ultraprecision $\mathcal{PT}$-symmetric QS on the trapped-ion platform. This work will provide theoretical guidance for the next stage of experimental efforts on the trapped-ion platform.

ACKNOWLEDGMENTS

This work is supported by the National Natural Science Foundation of China (Grants No. 11904402, No. 12074433, No. 12004430, No. 12174447, No. 12174448, and No. 12365006). Y.Y.W. acknowledges support from the Youth Program of the Natural Science Foundation of Guangxi (Grant No. 2021GXNSFBA075049). Y.Y.W. thanks Professor Mao-Fa Fang for many helpful discussions.

APPENDIX A: MORE DETAILS OF SCHEME I

1. $\mathcal{PT}$-symmetric system

The $\mathcal{PT}$-symmetric Hamiltonian primarily considered in this paper is

$$H_{\mathcal{PT}} = \frac{\omega}{2}\sigma_x + \mathrm{i}\frac{\gamma}{2}\sigma_z = \frac{\omega}{2}\begin{pmatrix} \mathrm{i}\gamma/\omega & 1 \\ 1 & -\mathrm{i}\gamma/\omega \end{pmatrix}. \quad \text{(A1)}$$

The ratio γ/ω is usually regarded as the non-Hermiticity in the system described by $H_{\mathcal{PT}}$. The spontaneous $\mathcal{PT}$-symmetry breaking is generated by the interplay of the tunable gain-loss rate γ and the coupling rate ω; when $\gamma/\omega \in (0, 1)$, $H_{\mathcal{PT}}$ is in the $\mathcal{PT}$-symmetric phase with real eigenvalues; while when $\gamma/\omega \in (1, \infty)$, $H_{\mathcal{PT}}$ is in the $\mathcal{PT}$-symmetry broken phase with a pair of complex conjugate eigenvalues. And $\gamma/\omega = 1$ usually represents the EP of $H_{\mathcal{PT}}$, at which the eigenvalues transition from being real to complex conjugate, accompanied by the degeneracy of the eigenstates. When $\gamma = 0$, representing an absence of non-Hermiticity, the $\mathcal{PT}$-symmetric system degrades into a (Hermitian) Rabi oscillator with coupling rate ω. Based on the eigenvalue equation,

$$H_{\mathcal{PT}}|\mathrm{E}_\pm\rangle = \mathrm{E}_\pm|\mathrm{E}_\pm\rangle, \quad \text{(A2a)}$$

the eigenvalues of $H_{\mathcal{PT}}$ are given by

$$\mathrm{E}_\pm = \pm\kappa/2, \quad \text{(A2b)}$$

where $\kappa = \sqrt{\omega^2 - \gamma^2}$. According to the standard Dirac inner product $\langle \mathrm{E}_\pm|\mathrm{E}_\mp\rangle = 0$, the orthogonal eigenvectors are given as

$$|\mathrm{E}_\pm\rangle = \frac{1}{\omega}\begin{pmatrix} \mathrm{i}\gamma \pm \kappa \\ \omega \end{pmatrix}. \quad \text{(A2c)}$$

Non-Hermitian Hamiltonians ($H_{\mathrm{NH}} \neq H_{\mathrm{NH}}^\dagger$) always can be decomposed into Hermitian and anti-Hermitian parts as

$H_{\rm NH} = H_+ + H_-$ with $H_\pm = \pm H_\pm^\dagger$. We decompose the $\mathcal{PT}$-symmetric Hamiltonian $H_{\mathcal{PT}}$ in Eq. (A1) into

$$H_+ = \frac{\omega}{2}\sigma_x;\ H_- = -\mathrm{i}\Gamma = \mathrm{i}\frac{\gamma}{2}\sigma_z, \tag{A3}$$

and solve the NH dynamics equation [59]

$$\dot{\rho}_t = -\mathrm{i}[H_+, \rho_t] - \{\Gamma, \rho_t\} + 2\mathrm{Tr}(\rho_t\Gamma)\rho_t. \tag{A4}$$

However, the NH dynamics Eq. (A4) for a normalized ρ_t is usually hard to solve analytically. Its solution can also be expressed as a unitarylike form:

$$\rho_t = \frac{U_{\mathcal{PT}}\rho_0 U_{\mathcal{PT}}^\dagger}{\mathrm{Tr}(U_{\mathcal{PT}}\rho_0 U_{\mathcal{PT}}^\dagger)} = \begin{pmatrix}\rho_t^{11} & \rho_t^{12}\\ \rho_t^{21} & \rho_t^{22}\end{pmatrix}, \tag{A5}$$

where $U_{\mathcal{PT}} = \exp(-\mathrm{i}H_{\mathcal{PT}}t)$ is the nonunitary time-evolution operator of the $\mathcal{PT}$-symmetric system and ρ_0 is an arbitrary initial state. Considering an initial pure state $\rho_0 = |\psi_0\rangle\langle\psi_0|$,

$$|\psi_0\rangle = a_0|1\rangle + b_0|2\rangle = \begin{pmatrix}a_0\\ b_0\end{pmatrix}, \tag{A6}$$

the solution in Eq. (A5) can be reduced to

$$|\psi_t\rangle = \frac{U_{\mathcal{PT}}|\psi_0\rangle}{\sqrt{\langle\psi_0|U_{\mathcal{PT}}^\dagger U_{\mathcal{PT}}|\psi_0\rangle}} = \mathrm{c_n}U_{\mathcal{PT}}|\psi_0\rangle$$
$$= a_t|1\rangle + b_t|2\rangle = \begin{pmatrix}a_t\\ b_t\end{pmatrix}, \tag{A7a}$$

where

$$a_t = \mathrm{c_n}\left[a_0\cos\left(\frac{\kappa t}{2}\right) + \frac{1}{\kappa}(a_0\gamma - \mathrm{i}b_0\omega)\sin\left(\frac{\kappa t}{2}\right)\right];$$
$$b_t = \mathrm{c_n}\left[b_0\cos\left(\frac{\kappa t}{2}\right) - \frac{1}{\kappa}(b_0\gamma + \mathrm{i}a_0\omega)\sin\left(\frac{\kappa t}{2}\right)\right], \tag{A7b}$$

and the renormalized factor $\mathrm{c_n}$ is given by

$$\frac{1}{\mathrm{c_n}^2} = \mathrm{Tr}(U_{\mathcal{PT}}|\psi_0\rangle\langle\psi_0|U_{\mathcal{PT}}^\dagger) = \langle\psi_0|U_{\mathcal{PT}}^\dagger U_{\mathcal{PT}}|\psi_0\rangle$$
$$= \left[b_0\cos\left(\frac{\kappa t}{2}\right) - \frac{1}{\kappa}(\mathrm{i}a_0\omega + b_0\gamma)\sin\left(\frac{\kappa t}{2}\right)\right]$$
$$\times\left[b_0^*\cos\left(\frac{\kappa t}{2}\right) + \frac{1}{\kappa}(\mathrm{i}a_0^*\omega - b_0^*\gamma)\sin\left(\frac{\kappa t}{2}\right)\right]$$
$$+\left[a_0\cos\left(\frac{\kappa t}{2}\right) + \frac{1}{\kappa}(a_0\gamma - \mathrm{i}b_0\omega)\sin\left(\frac{\kappa t}{2}\right)\right]$$
$$\times\left[a_0^*\cos\left(\frac{\kappa t}{2}\right) + \frac{1}{\kappa}(a_0^*\gamma + \mathrm{i}b_0^*\omega)\sin\left(\frac{\kappa t}{2}\right)\right]. \tag{A7c}$$

The corresponding density operator ρ_t in Eq. (A5) can be represented as

$$\rho_t = |\psi_t\rangle\langle\psi_t| = \begin{pmatrix}a_t\\ b_t\end{pmatrix}(a_t^*\ b_t^*), \tag{A8a}$$

and the matrix elements of normalized ρ_t are

$$\rho_t^{11} = |a_t|^2;\ \rho_t^{22} = 1 - \rho_t^{11} = |b_t|^2;$$
$$\rho_t^{12} = a_t b_t^*;\ \rho_t^{21} = \left(\rho_t^{12}\right)^* = b_t a_t^*. \tag{A8b}$$

The initial state in this paper is chosen as

$$|\psi_0\rangle = |+\rangle_y = \frac{\sqrt{2}}{2}\begin{pmatrix}1\\ \mathrm{i}\end{pmatrix}, \tag{A9}$$

i.e., $a_0 = 1/\sqrt{2}$; $b_0 = \mathrm{i}/\sqrt{2}$, where $|\pm\rangle_y = (|1\rangle \pm \mathrm{i}|2\rangle)/\sqrt{2}$ are the eigenvectors of the Pauli matrix σ_y.

Scheme I: Naimark-dilated quantum system. We now discuss quantum simulating the $\mathcal{PT}$-symmetric Hamiltonian through introducing an auxiliary system. Utilizing the Naimark-dilation theory, embedding the $\mathcal{PT}$-symmetric subspace into a larger Hermitian space with an auxiliary subspace, the $\mathcal{PT}$-symmetric nonunitary dynamics can be mapped from a unitary dynamics in the enlarged system, and the process is decomposed into the following two steps.

Step 1: Utilizing the Naimark-dilation theory. Constructing a Hermitian metric operator $\eta = \eta^\dagger$ based on the pseudo-Hermiticity condition [9]:

$$\eta H_{\mathcal{PT}} = (\eta H_{\mathcal{PT}})^\dagger = H_{\mathcal{PT}}^\dagger\eta^\dagger = H_{\mathcal{PT}}^\dagger\eta. \tag{A10}$$

With the basis $\{|i\rangle\}$ $(i = 1, 2, 3, 4)$, the $\mathcal{PT}$-symmetric subsystem ($\mathcal{PT}$-sub) $|\psi_t\rangle$ is denoted with $\{|1\rangle, |2\rangle\}$, and the auxiliary subsystem ($\mathcal{A}$-sub) $|\chi_t\rangle$ is denoted with $\{|3\rangle, |4\rangle\}$. According to the $\mathcal{PT}$ inner product [3],

$$(\mu, \nu) = (\mathcal{PT}\mu)\nu, \tag{A11}$$

where $\mathcal{P} = \sigma_x$ is the parity operator and $\mathcal{T}$ is the complex conjugate operator, the orthonormal eigenvectors $|E_\pm\rangle$ of $H_{\mathcal{PT}}$ are satisfied with $(E_\pm, E_\mp) = 0$ and

$$(E_\pm, E_\pm) = \pm 1, \tag{A12a}$$

while returning to $|\mathrm{E}_\pm\rangle$ according to the standard Dirac inner product given by Eq. (A2c):

$$(\mathrm{E}_\pm, \mathrm{E}_\pm) = (\mathcal{PT}|\mathrm{E}_\pm\rangle)|\mathrm{E}_\pm\rangle = \pm\frac{2\kappa}{\omega}, \tag{A12b}$$

and setting f as the normalized factor of transformation:

$$\frac{1}{f^2} = \frac{2\kappa}{\omega} \Longrightarrow f = \frac{1}{\sqrt{2\kappa/\omega}}. \tag{A13}$$

We arrange $|E_\pm\rangle = f|\mathrm{E}_\pm\rangle$ into the row matrix,

$$\Phi = (|E_+\rangle\ |E_-\rangle) = f(|\mathrm{E}_+\rangle\ |\mathrm{E}_-\rangle)$$
$$= \frac{1}{\sqrt{2\kappa\omega}}\begin{pmatrix}\mathrm{i}\gamma + \kappa & \mathrm{i}\gamma - \kappa\\ \omega & \omega\end{pmatrix}, \tag{A14}$$

and the metric operator is defined by

$$\eta = (\Phi\Phi^\dagger)^{-1} = \frac{\omega}{\kappa}\left(\mathbb{I} + \frac{\gamma}{\omega}\sigma_y\right)$$
$$= \frac{\omega}{\kappa}\begin{pmatrix}1 & -\mathrm{i}\gamma/\omega\\ \mathrm{i}\gamma/\omega & 1\end{pmatrix}. \tag{A15}$$

We regard the metric operator η as a synchronization link of dynamics between $\mathcal{A}$-sub [non-normalized $|\chi_t\rangle$] and $\mathcal{PT}$-sub [normalized $|\psi_t\rangle$ in Eq. (A7a)]:

$$|\chi_t\rangle = \eta|\psi_t\rangle = \begin{pmatrix}c_t\\ d_t\end{pmatrix}, \tag{A16a}$$

where

$$c_t = \frac{1}{\kappa}(\omega a_t - \mathrm{i}\gamma b_t);$$
$$d_t = \frac{1}{\kappa}(\mathrm{i}\gamma a_t + \omega b_t). \tag{A16b}$$

There are three serial perspectives for comprehending the dynamics of an enlarged Hermitian system: (a) constructing a total wave function of the enlarged Hermitian system by directly connecting the dynamics of $\mathcal{PT}$-sub and $\mathcal{A}$-sub by the synchronization link η as Eq. (A17); (b) figuring out the total unitary time-evolution operator of the enlarged Hermitian system and obtaining its purely unitary evolution processing as Eqs. (A18) and (A19); (c) expanding a Hermitian Hamiltonian to govern the dynamics of an enlarged Hermitian system such as Eq. (A20).

By embedding the $\mathcal{PT}$-symmetric space as a NH subspace $\mathcal{H}_{\mathcal{PT}}$ into a larger Hermitian space $\mathcal{H}_{\mathrm{H(4d)}} = \mathcal{H}_{\mathcal{PT}(2\mathrm{d})} \oplus \mathcal{H}_{\mathcal{A}(2\mathrm{d})}$ with an auxiliary subspace $\mathcal{H}_{\mathcal{A}}$ [4], and the wave function of the enlarged Hermitian system is constructed as

$$|\Psi_t\rangle = \mathrm{C_n}\left(\begin{bmatrix}1\\0\end{bmatrix}\otimes|\psi_t\rangle + \begin{bmatrix}0\\1\end{bmatrix}\otimes|\chi_t\rangle\right) = \mathrm{C_n}\begin{pmatrix}\psi_t\\ \chi_t\end{pmatrix} = (\tilde{a}_t\ \tilde{b}_t\ \tilde{c}_t\ \tilde{d}_t)^{\mathrm{T}}, \tag{A17a}$$

with the renormalized factor

$$\mathrm{C_n} = \frac{1}{\sqrt{\langle\psi_t|\psi_t\rangle + \langle\chi_t|\chi_t\rangle}} = \frac{1}{\sqrt{1+|c_t|^2+|d_t|^2}}, \tag{A17b}$$

elements of $|\Psi_t\rangle$ with $|\psi_0\rangle = |+\rangle_y$ are given as

$$\begin{aligned}
\tilde{a}_t &= \mathrm{c}_{4\mathrm{d}(+)}[\kappa\cos(\kappa t/2) + (\omega+\gamma)\sin(\kappa t/2)];\\
\tilde{b}_t &= \mathrm{i}\mathrm{c}_{4\mathrm{d}(-)}[(\omega-\gamma)\cos(\kappa t/2) - \kappa\sin(\kappa t/2)];\\
\tilde{c}_t &= \mathrm{c}_{4\mathrm{d}(+)}[(\omega+\gamma)\cos(\kappa t/2) + \kappa\sin(\kappa t/2)];\\
\tilde{d}_t &= \mathrm{i}\mathrm{c}_{4\mathrm{d}(-)}[\kappa\cos(\kappa t/2) - (\omega-\gamma)\sin(\kappa t/2)],
\end{aligned} \tag{A17c}$$

where $\mathrm{c}_{4\mathrm{d}(\pm)} = [4\omega(\omega\pm\gamma)]^{-1/2}$.

The unitary time evolution of the enlarged Hermitian system according to Eq. (A17) can also be expressed as

$$\begin{aligned}
|\Psi_t\rangle &= \mathrm{C_n}\begin{pmatrix}\psi_t\\ \chi_t\end{pmatrix} = \mathrm{C_n}\begin{pmatrix}\psi_t\\ \eta\psi_t\end{pmatrix} = \mathrm{C_n}\begin{pmatrix}\mathrm{c_n}(U_{\mathcal{PT}}\psi_0)\\ \mathrm{c_n}(\eta U_{\mathcal{PT}}\eta^{-1}\chi_0)\end{pmatrix}\\
&= \mathrm{C_n}\mathrm{c_n}\begin{pmatrix}U_{\mathcal{PT}} & 0\\ 0 & \eta U_{\mathcal{PT}}\eta^{-1}\end{pmatrix}\begin{pmatrix}\psi_0\\ \chi_0\end{pmatrix}\\
&= \tilde{\mathrm{C}}_{\mathrm{n}}\begin{pmatrix}U_{\mathcal{PT}} & 0\\ 0 & U_{\mathcal{A}}\end{pmatrix}\begin{pmatrix}\psi_0\\ \chi_0\end{pmatrix} = \tilde{\mathrm{C}}_{\mathrm{n}}U_{\mathrm{H}}\begin{pmatrix}\psi_0\\ \chi_0\end{pmatrix}\\
&= U_{4\mathrm{d}}|\Psi_0\rangle,
\end{aligned} \tag{A18a}$$

where $U_{\mathcal{A}} = \eta U_{\mathcal{PT}}\eta^{-1}$, with $U_{\mathcal{PT}} = \exp(-\mathrm{i}H_{\mathcal{PT}}t)$, and the purely unitary time-evolution operator of the enlarged Hermitian system is

$$U_{4\mathrm{d}} = (\mathrm{C_n}\mathrm{c_n})U_{\mathrm{H}} = \tilde{\mathrm{C}}_{\mathrm{n}}U_{\mathrm{H}}, \tag{A18b}$$

with the renormalized factor

$$\tilde{\mathrm{C}}_{\mathrm{n}} = 1/\sqrt{\langle\psi_0|U_{\mathcal{PT}}^{\dagger}U_{\mathcal{PT}}|\psi_0\rangle + \langle\chi_0|U_{\mathcal{A}}^{\dagger}U_{\mathcal{A}}|\chi_0\rangle}, \tag{A18c}$$

and the unitarylike U_{H} is directly obtained by applying the synchronization link of subsystems dynamics η:

$$U_{\mathrm{H}} = \begin{pmatrix}U_{\mathcal{PT}} & 0\\ 0 & U_{\mathcal{A}}\end{pmatrix} = \begin{pmatrix}U_{\mathcal{PT}} & 0\\ 0 & \eta U_{\mathcal{PT}}\eta^{-1}\end{pmatrix}. \tag{A18d}$$

With the Naimark-dilation theory, we have deduced the unitary time-evolution operator $U_{4\mathrm{d}}U_{4\mathrm{d}}^{\dagger} = \mathbb{I}$ related with the purely Hermitian Hamiltonian $H_{4\mathrm{d}} = H_{4\mathrm{d}}^{\dagger}$, which is obtained from $U_{4\mathrm{d}} = \exp(-\mathrm{i}H_{4\mathrm{d}}t)$. And the purely unitary evolution of the enlarged Hermitian system (denoted by the normalized density operator $\tilde{\rho}_{4\mathrm{d}}$) is represented as

$$\tilde{\rho}_{4\mathrm{d}} = |\Psi_t\rangle\langle\Psi_t| = U_{4\mathrm{d}}|\Psi_0\rangle\langle\Psi_0|U_{4\mathrm{d}}^{\dagger} = U_{4\mathrm{d}}\tilde{\rho}_0U_{4\mathrm{d}}^{\dagger}, \tag{A19a}$$

where $\tilde{\rho}_0 = |\Psi_0\rangle\langle\Psi_0|$ is the initial state related to $|\Psi_0\rangle = (\psi_0\ \chi_0)^{\mathrm{T}}$, here $|\chi_0\rangle = \eta|\psi_0\rangle$ is the initial state of $\mathcal{A}$-sub and $|\psi_0\rangle$ for $\mathcal{PT}$-sub given by Eq. (A9), and the matrix diagonal elements [i.e., population in $|i\rangle$ $(i = 1, 2, 3, 4)$] of normalized $\tilde{\rho}_{4\mathrm{d}}$ are

$$\begin{aligned}
\tilde{\rho}_{4\mathrm{d}}^{11} &= |\tilde{a}_t|^2 = [\omega - \gamma\cos(\kappa t) + \kappa\sin(\kappa t)]/4\omega;\\
\tilde{\rho}_{4\mathrm{d}}^{22} &= |\tilde{b}_t|^2 = [\omega - \gamma\cos(\kappa t) - \kappa\sin(\kappa t)]/4\omega;\\
\tilde{\rho}_{4\mathrm{d}}^{33} &= |\tilde{c}_t|^2 = [\omega + \gamma\cos(\kappa t) + \kappa\sin(\kappa t)]/4\omega;\\
\tilde{\rho}_{4\mathrm{d}}^{44} &= |\tilde{d}_t|^2 = 1 - (|\tilde{a}_t|^2 + |\tilde{b}_t|^2 + |\tilde{c}_t|^2)\\
&= [\omega + \gamma\cos(\kappa t) - \kappa\sin(\kappa t)]/4\omega,
\end{aligned} \tag{A19b}$$

and other matrix off-diagonal elements:

$$\begin{aligned}
\tilde{\rho}_{4\mathrm{d}}^{12} &= \left(\tilde{\rho}_{4\mathrm{d}}^{21}\right)^* = \mathrm{i}[\gamma - \omega\cos(\kappa t)]/4\omega;\\
\tilde{\rho}_{4\mathrm{d}}^{13} &= \left(\tilde{\rho}_{4\mathrm{d}}^{31}\right)^* = [\kappa + \omega\sin(\kappa t)]/4\omega;\\
\tilde{\rho}_{4\mathrm{d}}^{14} &= \left(\tilde{\rho}_{4\mathrm{d}}^{41}\right)^* = -\mathrm{i}[\kappa\cos(\kappa t) + \gamma\sin(\kappa t)]/4\omega;\\
\tilde{\rho}_{4\mathrm{d}}^{23} &= \left(\tilde{\rho}_{4\mathrm{d}}^{32}\right)^* = \mathrm{i}[\kappa\cos(\kappa t) - \gamma\sin(\kappa t)]/4\omega;\\
\tilde{\rho}_{4\mathrm{d}}^{24} &= \left(\tilde{\rho}_{4\mathrm{d}}^{42}\right)^* = [\kappa - \omega\sin(\kappa t)]/4\omega;\\
\tilde{\rho}_{4\mathrm{d}}^{34} &= \left(\tilde{\rho}_{4\mathrm{d}}^{43}\right)^* = -\mathrm{i}[\gamma + \omega\cos(\kappa t)]/4\omega.
\end{aligned} \tag{A19c}$$

Note that the unitary time evolution of the enlarged Hermitian system in this paper is directly characterized by connecting the dynamics of two subsystems with the synchronization link η. We have verified that this time-evolution process is consistent with that of Ref. [4], which proposed a unitary evolution governed by an expanded dimension Hamiltonian. The corresponding $H_{4\mathrm{d}}$ based on the $\mathcal{PT}$-symmetric system in this paper is

$$\begin{aligned}
H_{4\mathrm{d}} = {} & f^2[\mathbb{I}\otimes(H_{\mathcal{PT}}\eta^{-1} + \eta H_{\mathcal{PT}})]\\
& + f^2[\mathrm{i}\sigma_y\otimes(H_{\mathcal{PT}} - H_{\mathcal{PT}}^{\dagger})].
\end{aligned} \tag{A20}$$

Step 2: Executing the postselection. Considering the postselection performed on the enlarged Hermitian system, the success rate and failure rate of postselection are respectively denoted as

$$\begin{aligned}
p_{\mathrm{suc}} &= P_1 + P_2;\\
p_{\mathrm{fail}} &= 1 - p_{\mathrm{suc}} = P_3 + P_4,
\end{aligned} \tag{A21}$$

where $P_{i(t)} = \tilde{\rho}_{4\mathrm{d}}^{ii}$ $(i = 1, 2, 3, 4)$ is the population in $|i\rangle$ of the enlarged Hermitian system, and $\tilde{\rho}_{4\mathrm{d}}^{ii}$ are the matrix diagonal elements of $\tilde{\rho}_{4\mathrm{d}}$ in Eq. (A19b). The renormalized population for $\mathcal{PT}$-sub:

$$\tilde{P}_1 = \frac{P_1}{P_1+P_2} = \rho_{\mathcal{PT}}^{11};\ \ \tilde{P}_2 = \frac{P_2}{P_1+P_2} = \rho_{\mathcal{PT}}^{22}, \tag{A22a}$$

the corresponding renormalized population for $\mathcal{A}$-sub:

$$\tilde{P}_3 = \frac{P_3}{P_3+P_4} = \rho_{\mathcal{A}}^{11};\ \ \tilde{P}_4 = \frac{P_4}{P_3+P_4} = \rho_{\mathcal{A}}^{22}. \tag{A22b}$$

By executing the postselection on the enlarged system $\tilde{\rho}_{4d}$, if successful, $\tilde{\rho}_{4d}$ is degraded into the $\mathcal{PT}$-symmetric system $\rho_{\mathcal{PT}}$:

$$\rho_{\mathcal{PT}} = \rho_t = \frac{|\psi_t\rangle\langle\psi_t|}{\mathrm{Tr}(|\psi_t\rangle\langle\psi_t|)} = \begin{pmatrix} \rho_t^{11} & \rho_t^{12} \\ \rho_t^{21} & \rho_t^{22} \end{pmatrix}, \tag{A23a}$$

where ρ_t^{ij} $(i, j = 1, 2)$ of ρ_t in Eq. (A5) with $|\psi_0\rangle = |+\rangle_y$:

$$\begin{aligned} \rho_{\mathcal{PT}}^{11} &= \rho_t^{11} = \frac{1}{2}[1 + \mathrm{c_{pt}}\kappa \sin(\kappa t)]; \\ \rho_{\mathcal{PT}}^{12} &= \rho_t^{12} = \mathrm{i}\frac{\mathrm{c_{pt}}}{2}[\gamma - \omega\cos(\kappa t)]; \\ \rho_{\mathcal{PT}}^{21} &= \rho_t^{21} = \left(\rho_t^{12}\right)^* = -\mathrm{i}\frac{\mathrm{c_{pt}}}{2}[\gamma - \omega\cos(\kappa t)]; \\ \rho_{\mathcal{PT}}^{22} &= \rho_t^{22} = 1 - \rho_t^{11} = \frac{1}{2}[1 - \mathrm{c_{pt}}\kappa \sin(\kappa t)], \end{aligned} \tag{A23b}$$

where $\mathrm{c_{pt}} = [\omega - \gamma\cos(\kappa t)]^{-1}$; if it fails, $\tilde{\rho}_{4d}$ is degraded into the $\mathcal{A}$ system $\rho_{\mathcal{A}}$:

$$\rho_{\mathcal{A}} = \frac{|\chi_t\rangle\langle\chi_t|}{\mathrm{Tr}(|\chi_t\rangle\langle\chi_t|)} = \begin{pmatrix} \rho_t^{22} & \rho_t^{21} \\ \rho_t^{12} & \rho_t^{11} \end{pmatrix}, \tag{A24a}$$

where ρ_t^{ij} $(i, j = 1, 2)$ of ρ_t in Eq. (A5) with $|\psi_0\rangle = |-\rangle_y$:

$$\begin{aligned} \rho_{\mathcal{A}}^{11} &= \rho_t^{22} = \frac{1}{2}[1 + \mathrm{c_a}\kappa \sin(\kappa t)]; \\ \rho_{\mathcal{A}}^{12} &= \rho_t^{21} = -\mathrm{i}\frac{\mathrm{c_a}}{2}[\gamma + \omega\cos(\kappa t)]; \\ \rho_{\mathcal{A}}^{21} &= \rho_t^{12} = \left(\rho_t^{21}\right)^* = \mathrm{i}\frac{\mathrm{c_a}}{2}[\gamma + \omega\cos(\kappa t)]; \\ \rho_{\mathcal{A}}^{22} &= \rho_t^{11} = 1 - \rho_t^{22} = \frac{1}{2}[1 - \mathrm{c_a}\kappa \sin(\kappa t)], \end{aligned} \tag{A24b}$$

where $\mathrm{c_a} = [\omega + \gamma\cos(\kappa t)]^{-1}$. Equations (A23) and (A24) indicate that because of the full synchronization link η with the $\mathcal{PT}$-sub, the $\mathcal{A}$-sub does indeed possess the feature of $\mathcal{PT}$ symmetry. In consequence, two subsystems possess an anti-mirror-symmetric correlation [see Figs. 2(e) and 2(f)], and the enlarged Hermitian system combined by two fully synchronized $\mathcal{PT}$-symmetric subsystems can be regarded as a pseudo-dual-$\mathcal{PT}$-symmetric system, and EPs of $\mathcal{PT}$-sub and $\mathcal{A}$-sub overlap at $\gamma/\omega = 1$.

APPENDIX B: MORE DETAILS OF SCHEME II

Scheme II: Effective non-Hermitian Hamiltonian of open quantum system. Here we discuss quantum simulating the $\mathcal{PT}$-symmetric Hamiltonian by introducing an external environment. As we know, the dynamics of open quantum systems obey the Lindblad master equation [74],

$$\dot{\rho}_t = \mathcal{L}\rho_t, \tag{B1a}$$

with the dynamics generator $\mathcal{L}$, which is an arbitrary, linear or nonlinear, Liouvillian superoperator,

$$\mathcal{L}(\cdot) \equiv -\mathrm{i}[H_0, (\cdot)] + \mathcal{D}(\cdot), \tag{B1b}$$

and the dissipator $\mathcal{D}(\cdot)$ is defined by the Lindbladian

$$\mathcal{D}(\cdot) = J(\cdot)J^\dagger - \frac{1}{2}\{J^\dagger J, (\cdot)\}, \tag{B1c}$$

where $J(\cdot)J^\dagger$ represents the quantum jump term with the quantum jump operator J, and $\{J^\dagger J, (\cdot)\}$ denotes the coherent nonunitary dissipation terms.

Method 1: Effective rule and renormalization. In order to study the $\mathcal{PT}$-symmetric system with $H_{\mathcal{PT}}$, consider a dissipative two-level system described by an NH Hamiltonian H_{eff} with the Hilbert eigenvector basis $\{|i\rangle\}_{\mathcal{H}}$ $(i = 1, 2)$:

$$\begin{aligned} H_{\mathrm{eff}} &= \frac{\omega}{2}\sigma_x - \mathrm{i}\gamma\,|2\rangle\langle 2| = H_{\mathcal{PT}} - \mathrm{i}\frac{\gamma}{2}\mathbb{I} \\ &= \frac{\omega}{2}\begin{pmatrix} 0 & 1 \\ 1 & -\mathrm{i}2\gamma/\omega \end{pmatrix}, \end{aligned} \tag{B2}$$

where ω is the coupling rate, γ is the tunable decay rate, and EPs of H_{eff} and $H_{\mathcal{PT}}$ overlap at $\gamma/\omega = 1$.

First, such a dissipative two-level system can also be regarded as an effective description of a three-level system based on the perturbation approximation, with the basis $\{|i\rangle\}_{\mathcal{H}}$ $(i = 1, 2, 3)$, where the coherent transition is denoted by $|1\rangle \leftrightarrow |2\rangle$ with the coupling rate ω, the dissipation of the two-level system is represented by $|2\rangle \to |3\rangle$ with the tunable decay rate γ, and there is no transition between $|1\rangle \nleftrightarrow |3\rangle$. The dynamics of the three-level system can be described by the Lindblad master equation with a Liouvillian superoperator $\mathcal{L}$:

$$\begin{aligned} \dot{\varrho}_t &= \mathcal{L}\varrho_t = -\mathrm{i}[H_0, \varrho_t] + \mathcal{D}\varrho_t \\ &= -\mathrm{i}\left[\frac{\omega}{2}\sigma_x, \varrho_t\right] + \left(J\varrho_t J^\dagger - \frac{1}{2}\{J^\dagger J, \varrho_t\}\right), \end{aligned} \tag{B3}$$

where ϱ_t is the normalized density operator of the three-level system, $H_0 = \omega\sigma_x/2$ is the coherent transition Hamiltonian, and $J = \sqrt{\gamma}\,|3\rangle\langle 2|$ is the quantum jump operator. Through solving the Lindblad master Eq. (B3) with the initial state $|\tilde{\psi}_0\rangle = |\tilde{+}\rangle_y = (|1\rangle + \mathrm{i}|2\rangle + 0|3\rangle)/\sqrt{2}$ and $\tilde{\varrho}_0 = |\tilde{\psi}_0\rangle\langle\tilde{\psi}_0|$, we can obtain the density operator ϱ_t and its matrix elements:

$$\begin{aligned} \varrho_t^{11} &= \mathrm{c_{3L}}[\omega - \gamma\cos(\kappa t) + \kappa\sin(\kappa t)]; \\ \varrho_t^{12} &= \mathrm{i}\mathrm{c_{3L}}[\gamma - \omega\cos(\kappa t)]; \\ \varrho_t^{21} &= \left(\varrho_t^{12}\right)^* = -\mathrm{i}\mathrm{c_{3L}}[\gamma - \omega\cos(\kappa t)]; \\ \varrho_t^{22} &= \mathrm{c_{3L}}[\omega - \gamma\cos(\kappa t) - \kappa\sin(\kappa t)]; \\ \varrho_t^{33} &= 1 - \left(\varrho_t^{11} + \varrho_t^{22}\right) = 1 - 2\mathrm{c_{3L}}[\omega - \gamma\cos(\kappa t)]; \\ \varrho_t^{13} &= \varrho_t^{31} = \varrho_t^{23} = \varrho_t^{32} = 0, \end{aligned} \tag{B4}$$

where $\mathrm{c_{3L}} = \mathrm{e}^{-\gamma t}[2(\omega - \gamma)]^{-1}$.

Secondly, according to the effective rule of open quantum systems, the dynamics generated by H_{eff} in Eq. (B2) can be depicted by reducing the dimension of Eq. (B3). This is accomplished by ignoring the quantum jumps and modifying the coherent nonunitary dissipation of $|2\rangle \to |3\rangle$ in the Lindbladian dissipator $\mathcal{D}\varrho_t$ to the decay term $-\mathrm{i}\gamma|2\rangle\langle 2|$ in the effective Hamiltonian H_{eff} with the loss rate γ, and then the lower-dimension Lindblad master equation without considering quantum jumps, can be used to describe the dynamics of dissipative two-level system:

$$\dot{\varrho}_{\mathrm{eff}} = \mathcal{L}\varrho_{\mathrm{eff}} = -\mathrm{i}[H_{\mathrm{eff}}, \varrho_{\mathrm{eff}}], \tag{B5a}$$

and the corresponding system of differential equations:

$$\begin{aligned}
\dot{\varrho}_{\rm eff}^{11} &= {\rm i}\omega\big(\varrho_{\rm eff}^{12} - \varrho_{\rm eff}^{21}\big)/2;\\
\dot{\varrho}_{\rm eff}^{12} &= {\rm i}\omega\big(\varrho_{\rm eff}^{11} - \varrho_{\rm eff}^{22}\big)/2 - \gamma\varrho_{\rm eff}^{12};\\
\dot{\varrho}_{\rm eff}^{21} &= {\rm i}\omega\big(\varrho_{\rm eff}^{22} - \varrho_{\rm eff}^{11}\big)/2 - \gamma\varrho_{\rm eff}^{21};\\
\dot{\varrho}_{\rm eff}^{22} &= {\rm i}\omega\big(\varrho_{\rm eff}^{21} - \varrho_{\rm eff}^{12}\big)/2 - 2\gamma\varrho_{\rm eff}^{22}.
\end{aligned} \tag{B5b}$$

We now deduce the corresponding matrix of superoperator $\mathcal{L}$ without quantum jumps with the Liouvillian eigenvector basis $\{\vec{\varrho}_l\}_{\mathcal{L}}$ $(l = 1, 2, 3, 4) \equiv \{\hat{\varrho}_l\} = \{|i\rangle\langle j|\}_{\mathcal{H}}$ $(i, j = 1, 2)$ based on a vectorized representation in Ref. [14]:

$$\mathcal{L} = \begin{pmatrix} 0 & {\rm i}\omega/2 & -{\rm i}\omega/2 & 0\\ {\rm i}\omega/2 & -\gamma & 0 & -{\rm i}\omega/2\\ -{\rm i}\omega/2 & 0 & -\gamma & {\rm i}\omega/2\\ 0 & -{\rm i}\omega/2 & {\rm i}\omega/2 & -2\gamma \end{pmatrix}, \tag{B6a}$$

and the eigenvalues $\mathrm{E}_{\mathcal{L}(i)}$ $(i = 1, 2, 3, 4)$ of $\mathcal{L}$ matrix are

$$\{\mathrm{E}_{\mathcal{L}(i)}\} = \{-\gamma \pm {\rm i}\kappa_{(1)(4)}, -\gamma_{(2)(3)}\}, \tag{B6b}$$

with the LEP $\gamma/\omega = 1$ coincided with the HEP of $H_{\mathcal{PT}}$, since the LEP of $\mathcal{L}$ without quantum jumps is exactly the same as the HEP of $H_{\rm eff}$ in Eq. (B2), along with $H_{\mathcal{PT}}$. The solution of Eq. (B5) equals the matrix elements of the lower-dimension ϱ_t in Eq. (B4):

$$\varrho_{\rm eff}^{ij} = \varrho_t^{ij},\ (i, j = 1, 2). \tag{B7}$$

The solution can also be simply expressed as

$$\varrho_{\rm eff} = U_{\rm eff}\varrho_0 U_{\rm eff}^{\dagger}, \tag{B8}$$

where $U_{\rm eff} = \exp(-{\rm i}H_{\rm eff}t)$ and $\varrho_0 = |\psi_0\rangle\langle\psi_0|$ with $|\psi_0\rangle = |+\rangle_y = (|1\rangle + {\rm i}|2\rangle)/\sqrt{2}$. In order to exactly simulate the characteristic of energy balance of gain and loss in the $\mathcal{PT}$-symmetric system, by directly adding a gain term ${\rm i}\gamma|1\rangle\langle 1|$ on $H_{\rm eff}$ of the dissipative two-level system whose energy is only with loss and without gain, the artificial $\mathcal{PT}$-symmetric system can be obtained:

$$\varrho_{\mathcal{PT}} = {\rm e}^{\gamma t}\varrho_{\rm eff}. \tag{B9}$$

Finally, by performing the renormalization on $\varrho_{\mathcal{PT}}$,

$$\rho_{\mathcal{PT}} = \frac{\varrho_{\mathcal{PT}}}{{\rm Tr}(\varrho_{\mathcal{PT}})} = \frac{{\rm e}^{\gamma t}\varrho_{\rm eff}}{{\rm Tr}({\rm e}^{\gamma t}\varrho_{\rm eff})} = \frac{\varrho_{\rm eff}}{{\rm Tr}(\varrho_{\rm eff})} = \rho_{\rm eff}, \tag{B10}$$

we then realize the construction of $\mathcal{PT}$-symmetric system $\rho_{\mathcal{PT}}$ governed by $H_{\mathcal{PT}}$ through the dissipative two-level system $\rho_{\rm eff}$ dominated by an effective NH Hamiltonian $H_{\rm eff}$.

Method 2: Postselection. From the perspective of the postselection techniques [24], after solving the Lindblad master Eq. (B3) and obtaining the density matrix ϱ_t of three-level system, we can also achieve $\mathcal{PT}$-symmetric system $\rho_{\mathcal{PT}}$ through directly performing the postselection on the three-level system ϱ_t:

$$\rho_{\mathcal{PT}} = \frac{1}{\varrho_t^{11} + \varrho_t^{22}}\begin{pmatrix} \varrho_t^{11} & \varrho_t^{12}\\ \varrho_t^{21} & \varrho_t^{22}\end{pmatrix} = \begin{pmatrix} \rho_t^{11} & \rho_t^{12}\\ \rho_t^{21} & \rho_t^{22}\end{pmatrix}, \tag{B11}$$

where ρ_t^{ij} $(i, j = 1, 2)$ of ρ_t in Eq. (A5) with $|\psi_0\rangle = |+\rangle_y$, and the success rate of postselection $p_{\rm suc} = \varrho_t^{11} + \varrho_t^{22}$ is actually denoted by the trace of $\varrho_{\rm eff}$ in Eq. (B7).

APPENDIX C: PARAMETER INFORMATION ENCODED IN PURE STATES

The SLD operator is denoted by $\partial_\omega\rho_\omega = (L_\omega\rho_\omega + \rho_\omega L_\omega)/2$ in Eq. (19), and QFI $\mathcal{F}_\omega = {\rm Tr}(\rho_\omega L_\omega^2)$ in Eq. (20a) for the parameters is simply the diagonal element of the QFI matrix [66], which consists of only one element for single-parameter estimation. With the spectral decomposition $\rho_\omega = \sum_{n=1}^{N}\varepsilon_n|\psi_n\rangle\langle\psi_n|$, where ε_n and $|\psi_n\rangle$ are the nth eigenvalue and eigenstate of the full-rank density matrix ρ_ω, and $N = \dim\rho_\omega$. The derivative of ρ_ω with respect to the estimated parameter ω can be expressed as

$$\begin{aligned}
\partial_\omega\rho_\omega = \sum_n &(\partial_\omega\varepsilon_n|\psi_n\rangle\langle\psi_n| + \varepsilon_n|\partial_\omega\psi_n\rangle\langle\psi_n|\\
&+ \varepsilon_n|\psi_n\rangle\langle\partial_\omega\psi_n|).
\end{aligned} \tag{C1}$$

Based on Eqs. (19) and (C1),

$$\begin{aligned}
\langle\psi_n|\partial_\omega\rho_\omega|\psi_m\rangle &= \tfrac{1}{2}(\varepsilon_n + \varepsilon_m)\langle\psi_n|L_\omega|\psi_m\rangle\\
&= \partial_\omega\varepsilon_n\delta_{nm} + \varepsilon_m\langle\psi_n|\partial_\omega\psi_m\rangle + \varepsilon_n\langle\partial_\omega\psi_n|\psi_m\rangle.
\end{aligned} \tag{C2}$$

Utilizing $\langle\psi_n|\partial_\omega\psi_m\rangle = -\langle\partial_\omega\psi_n|\psi_m\rangle$, we can obtain

$$\langle\psi_n|L_\omega|\psi_m\rangle = \delta_{nm}\frac{\partial_\omega\varepsilon_n}{\varepsilon_n} + \frac{2(\varepsilon_m - \varepsilon_n)}{\varepsilon_n + \varepsilon_m}\langle\psi_n|\partial_\omega\psi_m\rangle. \tag{C3}$$

Based on Eq. (C3) and the basis vector completeness, the definition Eq. (20a) can be decomposed into classical and quantum parts as $\mathcal{F}_\omega = \mathcal{F}_{\rm Q} + \mathcal{F}_{\rm C}$:

$$\begin{aligned}
\mathcal{F}_{\rm Q} &= \sum_n \frac{4\varepsilon_n(\varepsilon_m - \varepsilon_n)^2|\langle\psi_n|\partial_\omega\psi_m\rangle|^2}{(\varepsilon_n + \varepsilon_m)^2}\\
&= \sum_n 4\varepsilon_n\langle\partial_\omega\psi_n|\partial_\omega\psi_n\rangle - \sum_{n\neq m}\frac{8\varepsilon_n\varepsilon_m}{\varepsilon_n + \varepsilon_m}|\langle\partial_\omega\psi_n|\psi_m\rangle|^2;\\
\mathcal{F}_{\rm C} &= \sum_n \frac{(\partial_\omega\varepsilon_n)^2}{\varepsilon_n}.
\end{aligned} \tag{C4}$$

Thus, the qualitative difference in the impact on the precision of parameter estimation arises from whether the additional estimated-parameter information derived from the $\mathcal{A}$-system Eq. (A24) can be encoded in the parameterized state of the target $\mathcal{PT}$-symmetric system Eq. (A23).

In the case of the initial pure state $\rho_0 = |\psi_0\rangle\langle\psi_0|$,

$$\mathcal{F}_\omega = 4\langle\psi_0|\Delta^2 H_\omega|\psi_0\rangle \leqslant \|H_\omega\|^2 = (\varepsilon_\alpha - \varepsilon_\beta)^2 \equiv \mathcal{F}_{\rm Q}^{\rm c}, \tag{C5}$$

where $\langle\psi_0|\Delta^2 H_\omega|\psi_0\rangle$ represents the variance of the parameter generator $H_\omega = {\rm i}(\partial_\omega U_\omega)U_\omega^{\dagger}$ under the state $|\psi_0\rangle$, and $\|.\|$ is the seminorm. When $\varepsilon_{\alpha(\beta)}$ is the maximum (minimum) eigenvalue of H_ω, one can derive the channel QFI $\mathcal{F}_{\rm Q}^{\rm c}$ corresponding to the maximum QFI $\mathcal{F}_\omega^{\max}$ achievable by optimizing over all possible probe states. This derivation also demonstrates that the optimal probe (initial) state is always a pure state.

[1] C. M. Bender and S. Boettcher, Real spectra in non-Hermitian Hamiltonians having PT symmetry, Phys. Rev. Lett. **80**, 5243 (1998).

[2] C. M. Bender, Making sense of non-Hermitian Hamiltonians, Rep. Prog. Phys. **70**, 947 (2007).

[3] C. M. Bender, D. C. Brody, and H. F. Jones, Complex extension of quantum mechanics, Phys. Rev. Lett. **89**, 270401 (2002).

[4] U. Günther and B. F. Samsonov, Naimark-dilated PT-Symmetric brachistochrone, Phys. Rev. Lett. **101**, 230404 (2008).

[5] U. Günther and B. F. Samsonov, PT-symmetric brachistochrone problem, Lorentz boosts, and nonunitary operator equivalence classes, Phys. Rev. A **78**, 042115 (2008).

[6] S. Croke, PT-symmetric Hamiltonians and their application in quantum information, Phys. Rev. A **91**, 052113 (2015).

[7] K. Kawabata, Y. Ashida, and M. Ueda, Information retrieval and criticality in parity-time-symmetric systems, Phys. Rev. Lett. **119**, 190401 (2017).

[8] A. Mostafazadeh, Pseudo-Hermiticity versus PT-symmetry: The necessary condition for the reality of the spectrum of a non-Hermitian Hamiltonian, J. Math. Phys. **43**, 205 (2002).

[9] A. Mostafazadeh, Pseudo-Hermiticity versus PT-symmetry. II: A complete characterization of non-Hermitian Hamiltonians with a real spectrum, J. Math. Phys. **43**, 2814 (2002).

[10] N. Moiseyev, *Non-Hermitian Quantum Mechanics* (Cambridge University Press, Cambridge, England, 2011).

[11] R. El-Ganainy, K. G. Makris, M. Khajavikhan, Z. H. Musslimani, S. Rotter, and D. N. Christodoulides, Non-Hermitian physics and PT symmetry, Nat. Phys. **14**, 11 (2018).

[12] Y. Ashida, Z. Gong, and M. Ueda, Non-Hermitian physics, Adv. Phys. **69**, 249 (2020).

[13] M.-A. Miri and A. Alù, Exceptional points in optics and photonics, Science **363**, eaar7709 (2019).

[14] F. Minganti, A. Miranowicz, R. W. Chhajlany, and F. Nori, Quantum exceptional points of non-Hermitian Hamiltonians and Liouvillians: The effects of quantum jumps, Phys. Rev. A **100**, 062131 (2019).

[15] E. J. Bergholtz, J. C. Budich, and F. K. Kunst, Exceptional topology of non-Hermitian systems, Rev. Mod. Phys. **93**, 015005 (2021).

[16] W. D. Heiss, The physics of exceptional points, J. Phys. A: Math. Theor. **45**, 444016 (2012).

[17] W. Chen, Ş. K. Özdemir, G. Zhao, J. Wiersig, and L. Yang, Exceptional points enhance sensing in an optical microcavity, Nature (London) **548**, 192 (2017).

[18] B. Peng, Ş. K. Özdemir, S. Rotter, H. Yilmaz, M. Liertzer, F. Monifi, C. M. Bender, F. Nori, and L. Yang, Loss-induced suppression and revival of lasing, Science **346**, 328 (2014).

[19] H. Xu, D. Mason, L. Jiang, and J. G. E. Harris, Topological energy transfer in an optomechanical system with exceptional points, Nature (London) **537**, 80 (2016).

[20] B. Midya, H. Zhao, and L. Feng, Non-Hermitian photonics promises exceptional topology of light, Nat. Commun. **9**, 2674 (2018).

[21] A. Guo, G. J. Salamo, D. Duchesne, R. Morandotti, M. Volatier-Ravat, V. Aimez, G. A. Siviloglou, and D. N. Christodoulides, Observation of PT-symmetry breaking in complex optical potentials, Phys. Rev. Lett. **103**, 093902 (2009).

[22] Y. Wu, W. Liu, J. Geng, X. Song, X. Ye, C. K. Duan, X. Rong, and J. Du, Observation of parity-time symmetry breaking in a single-spin system, Science **364**, 878 (2019).

[23] J. Li, A. K. Harter, J. Liu, L. de Melo, Y. N. Joglekar, and L. Luo, Observation of parity-time symmetry breaking transitions in a dissipative Floquet system of ultracold atoms, Nat. Commun. **10**, 855 (2019).

[24] M. Naghiloo, M. Abbasi, Y. N. Joglekar, and K. W. Murch, Quantum state tomography across the exceptional point in a single dissipative qubit, Nat. Phys. **15**, 1232 (2019).

[25] Z.-P. Liu, J. Zhang, Ş. K. Özdemir, B. Peng, H. Jing, X.-Y. Lü, C.-W. Li, L. Yang, F. Nori, and Y.-X. Liu, Metrology with $\mathscr{P}\mathscr{T}$-symmetric cavities: Enhanced sensitivity near the $\mathscr{P}\mathscr{T}$-phase transition, Phys. Rev. Lett. **117**, 110802 (2016).

[26] A. McDonald and A. A. Clerk, Exponentially-enhanced quantum sensing with non-Hermitian lattice dynamics, Nat. Commun. **11**, 5382 (2020).

[27] Y. Chu, Y. Liu, H. Liu, and J. Cai, Quantum sensing with a single-qubit pseudo-Hermitian system, Phys. Rev. Lett. **124**, 020501 (2020).

[28] X.-W. Luo, C. Zhang, and S. Du, Quantum squeezing and sensing with pseudo-anti-parity-time symmetry, Phys. Rev. Lett. **128**, 173602 (2022).

[29] H. Hodaei, A. U. Hassan, S. Wittek, H. Garcia-Gracia, R. El-Ganainy, D. N. Christodoulides, and M. Khajavikhan, Enhanced sensitivity at higher-order exceptional points, Nature (London) **548**, 187 (2017).

[30] Y. H. Lai, Y. K. Lu, M. G. Suh, Z. Yuan, and K. Vahala, Observation of the exceptional-point-enhanced Sagnac effect, Nature (London) **576**, 65 (2019).

[31] J. Wiersig, Review of exceptional point-based sensors, Photon. Res. **8**, 1457 (2020).

[32] H. M. Wiseman and G. J. Milburn, *Quantum Measurement and Control* (Cambridge University Press, Cambridge, England, 2010).

[33] C. L. Degen, F. Reinhard, and P. Cappellaro, Quantum sensing, Rev. Mod. Phys. **89**, 035002 (2017).

[34] V. Giovannetti, S. Lloyd, and L. MacCone, Advances in quantum metrology, Nat. Photonics **5**, 222 (2011).

[35] S. Pirandola, B. R. Bardhan, C. W. T. Gehring, and S. Lloyd, Advances in photonic quantum sensing, Nat. Photonics **12**, 724 (2018).

[36] S. Yu, Y. Meng, J. S. Tang, X. Y. Xu, Y. T. Wang, P. Yin, Z. J. Ke, W. Liu, Z. P. Li, Y. Z. Yang, G. Chen, Y. J. Han, C. F. Li, and G. C. Guo, Experimental investigation of quantum PT-enhanced sensor, Phys. Rev. Lett. **125**, 240506 (2020).

[37] M. Saffman, T. G. Walker, and K. Mølmer, Quantum information with Rydberg atoms, Rev. Mod. Phys. **82**, 2313 (2010).

[38] T. M. Graham, Y. Song, J. Scott, C. Poole, L. Phuttitarn, K. Jooya, P. Eichler, X. Jiang, A. Marra, B. Grinkemeyer, M. Kwon, M. Ebert, J. Cherek, M. T. Lichtman, M. Gillette, J. Gilbert, D. Bowman, T. Ballance, C. Campbell, E. D. Dahl *et al.*, Multi-qubit entanglement and algorithms on a neutral-atom quantum computer, Nature (London) **604**, 457 (2022).

[39] C. D. Marciniak, T. Feldker, I. Pogorelov, R. Kaubruegger, D. V. Vasilyev, R. van Bijnen, P. Schindler, P. Zoller, R. Blatt, and T. Monz, Optimal metrology with programmable quantum sensors, Nature (London) **603**, 604 (2022).

[40] L. Ding, K. Shi, Q. Zhang, D. Shen, X. Zhang, and W. Zhang, Experimental determination of $\mathscr{P}\mathscr{T}$-symmetric exceptional

points in a single trapped ion, Phys. Rev. Lett. **126**, 083604 (2021).
[41] S. P. Wolski, D. Lachance-Quirion, Y. Tabuchi, S. Kono, A. Noguchi, K. Usami, and Y. Nakamura, Dissipation-based quantum sensing of magnons with a superconducting qubit, Phys. Rev. Lett. **125**, 117701 (2020).
[42] J. F. Barry, J. M. Schloss, E. Bauch, M. J. Turner, C. A. Hart, L. M. Pham, and R. L. Walsworth, Sensitivity optimization for NV-diamond magnetometry, Rev. Mod. Phys. **92**, 015004 (2020).
[43] B. Bürgler, T. F. Sjolander, O. Brinza, A. Tallaire, J. Achard, and P. Maletinsky, All-optical nuclear quantum sensing using nitrogen-vacancy centers in diamond, npj Quantum Inf. **9**, 56 (2023).
[44] J. C. Budich and E. J. Bergholtz, Non-Hermitian topological sensors, Phys. Rev. Lett. **125**, 180403 (2020).
[45] F. Koch and J. C. Budich, Quantum non-Hermitian topological sensors, Phys. Rev. Res. **4**, 013113 (2022).
[46] L. Bao, B. Qi, and D. Dong, Exponentially enhanced quantum non-Hermitian sensing via optimized coherent drive, Phys. Rev. Appl. **17**, 014034 (2022).
[47] S. Sarkar, F. Ciccarello, A. Carollo, and A. Bayat, Quantum-enhanced sensing from non-Hermitian topology, arXiv:2311.12756.
[48] L. Xiao, Y. Chu, Q. Lin, H. Lin, W. Yi, J. Cai, and P. Xue, Non-Hermitian sensing in the absence of exceptional points, arXiv:2403.08218.
[49] W. Langbein, No exceptional precision of exceptional point sensors, Phys. Rev. A **98**, 023805 (2018).
[50] C. Chen, L. Jin, and R. B. Liu, Sensitivity of parameter estimation near the exceptional point of a non-Hermitian system, New J. Phys. **21**, 083002 (2019).
[51] H. Wang, Y. H. Lai, Z. Yuan, M. G. Suh, and K. Vahala, Petermann-factor sensitivity limit near an exceptional point in a Brillouin ring laser gyroscope, Nat. Commun. **11**, 1610 (2020).
[52] J. Wiersig, Prospects and fundamental limits in exceptional point-based sensing, Nat. Commun. **11**, 2454 (2020).
[53] R. Duggan, S. A. Mann, and A. Alù, Limitations of sensing at an exceptional point, ACS Photon. **9**, 1554 (2022).
[54] H. K. Lau and A. A. Clerk, Fundamental limits and non-reciprocal approaches in non-Hermitian quantum sensing, Nat. Commun. **9**, 4320 (2018).
[55] M. Zhang, W. Sweeney, C. W. Hsu, L. Yang, A. D. Stone, and L. Jiang, Quantum noise theory of exceptional point amplifying sensors, Phys. Rev. Lett. **123**, 180501 (2019).
[56] R. Kononchuk, J. Cai, F. Ellis, R. Thevamaran, and T. Kottos, Exceptional-point-based accelerometers with enhanced signal-to-noise ratio, Nature (London) **607**, 697 (2022).
[57] H. A. Loughlin and V. Sudhir, Exceptional-point sensors offer no fundamental signal-to-noise ratio enhancement, arXiv:2401.04825.
[58] W. Ding, X. Wang, and S. Chen, Fundamental sensitivity limits for non-Hermitian quantum sensors, Phys. Rev. Lett. **131**, 160801 (2023).
[59] D. C. Brody and E.-M. Graefe, Mixed-state evolution in the presence of gain and loss, Phys. Rev. Lett. **109**, 230405 (2012).
[60] L. Xiao, K. Wang, X. Zhan, Z. Bian, K. Kawabata, M. Ueda, W. Yi, and P. Xue, Observation of critical phenomena in parity-time-symmetric quantum dynamics, Phys. Rev. Lett. **123**, 230401 (2019).
[61] W. Zhang, X. Ouyang, X. Huang, X. Wang, H. Zhang, Y. Yu, X. Chang, Y. Liu, D.-L. Deng, and L.-M. Duan, Observation of non-Hermitian topology with nonunitary dynamics of solid-state spins, Phys. Rev. Lett. **127**, 090501 (2021).
[62] X. Li, C. Zheng, J. Gao, and G. Long, Efficient simulation of the dynamics of an n-dimensional $\mathscr{P}\mathscr{T}$-symmetric system with a local-operations-and-classical-communication protocol based on an embedding scheme, Phys. Rev. A **105**, 032405 (2022).
[63] C.-W. Wu, M.-C. Zhang, Y.-L. Zhou, T. Chen, R. Huang, Y. Xie, B.-Q. Ou, W. Wu, A. Miranowicz, J. Zhang, H. Jing, and P.-X. Chen, Maximizing temporal quantum correlation by approaching an exceptional point, arXiv:2304.06590.
[64] W.-C. Wang, Y.-L. Zhou, H.-L. Zhang, J. Zhang, M.-C. Zhang, Y. Xie, C.-W. Wu, T. Chen, B.-Q. Ou, W. Wu, H. Jing, and P.-X. Chen, Observation of $\mathscr{P}\mathscr{T}$-symmetric quantum coherence in a single-ion system, Phys. Rev. A **103**, L020201 (2021).
[65] J. T. Barreiro, M. Müller, P. Schindler, D. Nigg, T. Monz, M. Chwalla, M. Hennrich, C. F. Roos, P. Zoller, and R. Blatt, An open-system quantum simulator with trapped ions, Nature (London) **470**, 486 (2011).
[66] J. Liu, H. Yuan, X.-M. Lu, and X. Wang, Quantum Fisher information matrix and multiparameter estimation, J. Phys. A **53**, 023001 (2020).
[67] W. Zhong, Z. Sun, J. Ma, X. Wang, and F. Nori, Fisher information under decoherence in Bloch representation, Phys. Rev. A **87**, 022337 (2013).
[68] Q. Zheng, L. Ge, Y. Yao, and Q.-J. Zhi, Enhancing parameter precision of optimal quantum estimation by direct quantum feedback, Phys. Rev. A **91**, 033805 (2015).
[69] L. J. Fiderer, J. M. E. Fraïsse, and D. Braun, Maximal quantum Fisher information for mixed states, Phys. Rev. Lett. **123**, 250502 (2019).
[70] J.-X. Peng, B. Zhu, W. Zhang, and K. Zhang, Dissipative quantum Fisher information for a general Liouvillian parameterized process, Phys. Rev. A **109**, 012432 (2024).
[71] E. Chitambar and G. Gour, Quantum resource theories, Rev. Mod. Phys. **91**, 025001 (2019).
[72] K. C. Tan, V. Narasimhachar, and B. Regula, Fisher information universally identifies quantum resources, Phys. Rev. Lett. **127**, 200402 (2021).
[73] Z. Chen and X. Hu, Resource theory of dephasing estimation in multiqubit systems, Phys. Rev. A **108**, 032415 (2023).
[74] H.-P. Breuer and F. Petruccione, *The Theory of Open Quantum Systems* (Oxford University Press, Oxford, UK, 2007).